Crystal Kayaro Emonde

MECHANICAL AND TRIBOLOGICAL BEHAVIOUR OF PEEK REINFORCED WITH SN-ZN-BI, SHORT CARBON FIBRES AND GRAPHENE NANOPLATELETS

VOLUME 1

Dissertação no âmbito do Mestrado Conjunto Europeu em tribologia de Superfícies e interfaces orientada pelos Professor/a Doutor/a (choose the title ot the supervisor) name of the supervisor> and Professor/a Doutor/a (choose the title ot the supervisor) name of the supervisor e apresentada ao Departamento de Engenharia Mecânica da Faculdade de Ciências e Tecnologia da Universidade de Coimbra.

Julho de 2021

1 2 9 0

FACULDADE DE CIÊNCIAS E TECNOLOGIA
UNIVERSIDADE D COIMBRA

Mechanical and tribological behaviour of PEEK reinforced with Sn-Zn-Bi, short carbon fibres and graphene nanoplatelets

Submitted in Partial Fulfilment of the Requirements for the Degree of European Joint European Master in Tribology of Surfaces and Interfaces.

Comportamento mecânico e tribológico de PEEK reforçado com Sn-Zn-Bi, fibras curtas de carbono e nanoplaquetas de grafeno

Author

Crystal Kayaro Emonde

Advisor[s]

Prof. Bruno Trindade

Dr. Emilio Frutos

Jury

President	**Prof. Albano Cavaleiro** **Professor at University of Coimbra**
Vowel	**Dr. Ricardo Serra** **Researcher at University of Coimbra**
Advisor	**Dr. Emilio Frutos** **Researcher at Instituto Pedro Nunes**

---

1 2 9 0
UNIVERSIDADE D COIMBRA

tribos

Coimbra, Julho de 2021

ACKNOWLEDGEMENTS

I wish to express my gratitude to my master thesis advisor Prof. Bruno Trindade from the University of Coimbra, for his professional support, guidance, and insightful suggestions during the writing of this work.

In addition, I would like to thank my assistant advisor, Dr Emilio Frutos, from Instituto Pedro Nunes (Coimbra), for his consistent support and guidance with the experimental section and writing of this work.

I would like to extend my gratitude to the staff at IPN, particularly to Mr Carlos Patacas, Mr Vitor Redonde, and Mr Nelson Duarte, for their time and effort in performing the characterisation of the project samples. Additionally, I would like to thank the staff at the Mechanical Department of the University of Coimbra particularly, Dr Manuel Evaristo, for his time and assistance with the nanomechanical characterisation performed on the samples.

Special thanks to the staff at the University of Aveiro who were a part of this work initially. I would like to particularly thank Dr Florinda Costa for providing the laser machine and expertise for the conduction of the initial texturing experiments.

Finally, I am thankful to the European Commission and the TRIBOS consortium for funding my master's studies. Without their financial support, the conduction of this thesis would not have been possible.

Abstract

Polyetheretherketone (PEEK) has shown great potential as a bearing material against metallic and ceramic components in orthopaedic implants. The advantage of PEEK over conventional polymers such as polyethylene (PE) and ultra-high molecular weight polyethylene (UHMWPE) lies in the fact that it has excellent thermal stability, is chemically resistant in corrosive environments, and possesses superior mechanical properties. Furthermore, PEEK has presented advantages over metallic implants due to its lower stiffness (~3-4 GPa), which could help mitigate bone resorption. However, studies have demonstrated that pure PEEK has a low wear resistance when compared to these polymers, which is an undesirable property in joint implants. As a result, PEEK composites have been explored, which have demonstrated significantly improved mechanical and tribological properties, closer in range and comparable to conventionally used polymers.

The aim of this study was to evaluate the effect of reinforcing PEEK with short carbon fibres (SCF) and graphene nanoplatelets (GNP) embedded in a soft Sn-based brazing alloy. Four composite mixtures composed of 67wt.% of PEEK and 33wt.% of varying concentrations of the reinforcements were made by mechanical alloying (MA). The reinforcement consisted of a fixed content of 89Sn-8Zn-3Bi wt.% and 3.3wt.% SCF whiskers with GNP being varied between; 0, 0.99, 2.31, and 4.95wt.%. The mechanical and tribological properties of these composites were compared with those of pure PEEK powder and commercially obtained PEEK.

Mechanical and tribological tests showed that the incorporation of these reinforcements in the PEEK matrix resulted in enhanced mechanical and tribological performance compared to unfilled PEEK. Furthermore, the incorporation of different contents of GNP, particularly 0.99wt.% resulted in a reduction of wear of PEEK by three times. It was concluded that the reduction of friction and wear was dependent upon the concentration of GNP added to the polymer matrix.

Keywords PEEK, short carbon fibres, graphene nanoplatelets, composite, mechanical alloying, compaction.

Resumo

O PEEK (poliéteretercetona) tem mostrado potencial para ser um material alternativo à utilização de materiais metálicos e cerâmicos em implantes ortopédicos. A vantagem do PEEK sobre os polímeros convencionais reside no facto de ter uma excelente estabilidade térmica, ser quimicamente resistente e possuir melhores propriedades mecânicas e tribológicas. Para além, o seu reforço com outras classes de materiais permite obter ainda melhores valores destas propriedades, especialmente quando comparados com os dos polímeros tradicionais. Tal é de extrema importância, já que o afrouxamento asséptico que ocorre devido ao desgaste dos componentes é a principal causa de falha dos implantes.

O objetivo deste estudo foi avaliar o efeito do de um reforço compósito constituído por uma liga de brasagem suave composta por Sn-Zn-Bi + fibras de carbono (SCF) e nanoplaquetas de grafeno (GNP) no desempenho tribológico do PEEK. Quatro misturas compostas de 67 wt.% de PEEK e 33 wt.% de reforço foram produzidas por síntese mecânica (MA). A liga de brasagem tinha a composição Sn89-Zn8-Bi3 %pd., o teor de SCF foi de 3,3 % pd. e o de GNP de 0, 0,99, 2,31, e 4,95 %pd. As propriedades mecânicas e tribológicas destes compósitos foram comparadas com as do PEEK prensado a partir de pó e do PEEK obtido comercialmente.

Os testes mecânicos e tribológicos mostraram que a incorporação destes reforços na matriz de PEEK resultou num melhor desempenho mecânico e tribológico em comparação com o PEEK não preenchido. Além disso, a incorporação de diferentes conteúdos de GNP e particularmente 0,99 %pd. resultou numa redução do desgaste de PEEK em três vezes. Concluiu-se ainda que a redução do atrito e do desgaste depende da concentração do teor de grafeno adicionado à matriz polimérica.

Palavras-chave: PEEK, fibras curtas de carbono (SCF), nanoplaquetas de grafeno (GNP), compósito, síntese mecânica, consolidação.

Table of contents

List of Figures

List of tables

Abbreviations and acronyms

Abbreviation	Meaning
CF	Carbon fibre
CFR	Carbon fibre reinforcement
CoF	Coefficient of friction
DSC	Differential scanning calorimetry
EDS	Electron dispersive spectroscopy
GNP	Graphene nanoplatelets
LST	Laser surface texturing
LVM	Low vacuum melting
MA	Mechanical alloying
MA'ed	Mechanically alloyed
OA	Osteoarthritis
PCA	Process control agent
PE	Polyethylene
PEEK	Polyether ether ketone
PMC	Polymer matrix composite
SA	Stearic acid
SCF	Short carbon fibres
SEM	Scanning Electron Microscopy
SS	Stainless steel
THA	Total hip arthroplasty
TJR	Total joint replacement
TKA	Total knee arthroplasty
UHMWPE	Ultra-high molecular weight polyethylene
WR	Wear rate
XRD	X-Ray diffraction

1. Introduction

The rise in ageing population, increase in obesity and sedentary lifestyles are some of the underlying factors behind the increase in osteoarthritis (OA) worldwide [1]. Many patients who are diagnosed with OA wish to maintain an active lifestyle for many more years, even after diagnosis [2]. Currently, total joint replacement (TJR) is the main treatment used to relieve moderate to severe OA cases, which cannot be treated through non-surgical procedures[1].

TJR is among the most successful and cost-effective surgical procedures performed clinically, with total knee arthroplasty (TKA) and total hip arthroplasty (THA) being the two most popular surgeries. These procedures are carried out in an attempt to relieve pain, as well as restore mobility and function in patients [3, 4]. Despite the success of these procedures, many patients still experience post-surgical pain, infection and some degree of functional limitation after surgery, which has driven the need for more research in this field [2].

One of the primary causes of implant failure results from wear debris released from the implant [5]. Aggregation of these wear particles stimulates cell reactions, i.e. cell activation, cytokine release and hypersensitive reaction, which lead to osteolysis, aseptic loosening and the eventual failure of the implant [6].

In the last few years, a significant number of materials have been used to reduce the debris released between the sliding surfaces in contact in the hip and knee joints. These include metals, ceramics and polymers arranged in various configurations such as hard-on-soft and hard-on-hard bearings, where soft bearings represent polymers and hard bearings represent metals and ceramics [7]. Materials usually employed to date include metallic alloys of titanium such as Ti6Al4V, CoCr (cobalt-chromium) alloys such as CoNiCrMo [8] and stainless steel (SS) 316 LVM (Low Vacuum Melting) [8]. Ceramic materials, such as alumina (Al_2O_3) and zirconia (ZrO_2), have mainly been used as bearing surfaces or as bone cement to improve bonding [8, 9].

Nevertheless, some patients have experienced hypersensitivity as a result of the release of ions from the metallic debris into the body when metal-metal articulated implants have been used [9]. On the other hand, the debris released from metal-ceramic and ceramic-ceramic combinations has shown less harmful effects on the body. However, the high cost and brittle nature of ceramic materials make them undesirable for being used in hip and knee replacement [2].

Since its introduction in the 1960s, ultra-high molecular weight polyethylene (UHMWPE) has been a “gold standard material” for use in hard-on-soft configurations due to its high wear resistance and chemical stability [10]. However, wear debris from UHMWPE implants, and its susceptibility to oxidation have been linked to severe osteolysis and implant loosening [5]. To improve the wear resistance of UHMWPE, crosslinking through radiation sterilisation was introduced in the 1990s. Unfortunately, the radiation had detrimental effects on the mechanical properties of UHMWPE, as it caused the introduction of free radicals into the material, making it susceptible to oxidation [11]. In spite of the problems associated with polyethylene (PE), UHMWPE remains the most widely used polymer in the manufacture of orthopaedic implants because it is cheap and easy to manufacture [12].

After its commercialisation in the 1980s and confirmation of its biocompatibility, Polyether ether ketone (PEEK) has been increasingly used as a biomaterial for the manufacture of

implants. PEEK is a semi-crystalline thermoplastic with excellent thermal stability, good chemical resistance and good mechanical properties as well as tribological properties [13]. In biomedical applications, PEEK is used as a structural material in stems of joints, intervertebral spacers, spinal cage implants, cervical disc replacements, replacement heart valves, dental implants etc. Furthermore, PEEK and its carbon fibre (CF) composites have been researched as bearing materials for TJR since the 90s [5] due to their low debris rate release, which is comparable to metal-on-metal bearings; high resistance to chemical damage, and ease of manufacture, which makes it an ideal implantable biomaterial to be used in the design of new hip and knee implants [3, 5].

Despite its low wear rate, pure PEEK has a relatively high CoF when compared with other polymers such as PE and UHMWPE [14]. For this reason, several PEEK composites have been developed to enhance its properties, in particular, mechanical strength and wear resistance, by reinforcing the polymer with different fillers depending on the desired property [15].

2. Motivation

This project aims to enhance the mechanical and tribological properties of PEEK polymer so as to improve its performance as a bearing and/or bushing material for TJR. This will be achieved through the design of a self-lubricating reinforced PEEK composite, with low friction and low wear rate, capable of minimising the formation and release of debris. The friction and wear properties of the composite will be evaluated in comparison with unfilled PEEK under identical test conditions.

Initially, this work was to be done through laser texturing of the PEEK surface to develop a grid pattern. The self-lubricating reinforcement would be introduced and sintered by a laser. Initial laser texturing experiments were done on commercial PEEK samples in collaboration with the University of Aveiro. However, due to unexpected circumstances with the laser, the design and fabrication method of the composite was changed and mechanical alloying selected as the final processing route.

3. State of the art

3.1. Composite materials

Composites are materials made of two or more materials, where one of them acts as a matrix and the rest as fillers [16]. These materials are combined together in a certain order, on a macroscopic level, to form a new material with improved properties not inherent to the raw materials. Depending on the user's requirements, the new properties may be mechanical, optical, magnetic, etc.

Composites are generally classified into three categories, namely:

- Polymer Matrix Composites (PMCs)
- Metal Matrix Composite (MMCs)
- Ceramic Matrix Composites (CMCs)

based on the matrix material [16].

3.1.1. Polymer Matrix Composites

PMCs are multiphase solid materials that consist of a polymer matrix and filler/reinforcement material, which possess substantially different or better properties than the polymer itself [16].

The type of reinforcement used for PMCs may be classified into three groups, i.e., particulates (e.g., nanoparticles), short fibres or whiskers (e.g., cellulose, carbon fibres, etc.) and layers or sheets (e.g., graphene). The choice of reinforcement depends on the desired properties as well as the application of the polymer. This could range from enhanced mechanical, tribological, thermal properties, among others [16].

The biggest challenge in the fabrication of PMCs is ensuring that the reinforcement was uniformly dispersed within the polymer matrix and that there is good integration between the matrix and reinforcement [17].

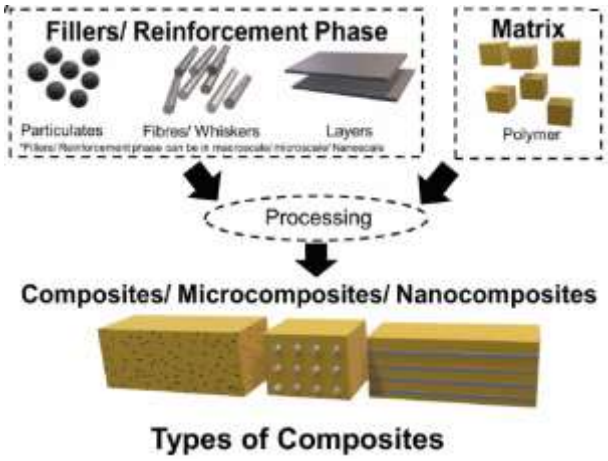

Figure 1. Illustration of the fabrication of a polymer composite [18].

The two conventional methods used to fabricated PMCs are solvent casting and melt blending [19].

Solvent casting

This technique involves dissolving one or more reinforced polymers in the form of powders in a solvent in which the polymers are completely or partially soluble. After that, the solvent is evaporated, and the final mixture of reinforced powders is dried in an oven. Finally, they are compacted and sintered. The particularity of this processing route is related to the type of solvent used since this affects the resulting mechanical and physical properties of the compound [18].

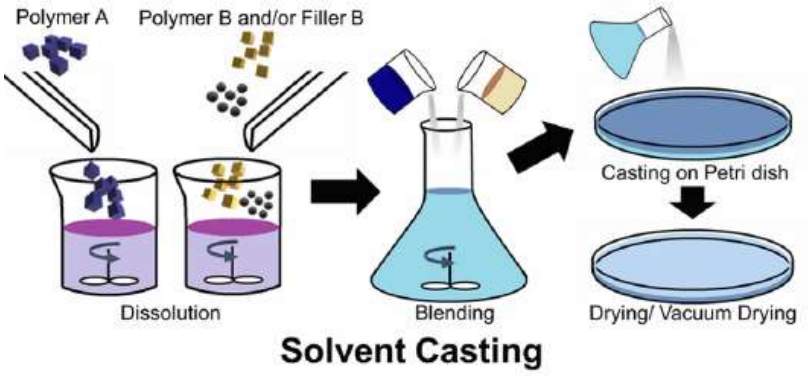

Figure 2. Illustration of solvent blending process [18].

Melt blending/ Injection moulding

In melt blending, the polymer is melted and reinforcement added to it, after which they are continuously blended together. Once blended, the composite is extruded and cooled. The disadvantage of this method is that it is limited to thermoplastics as many natural polymers would deteriorate before melting occurs [18].

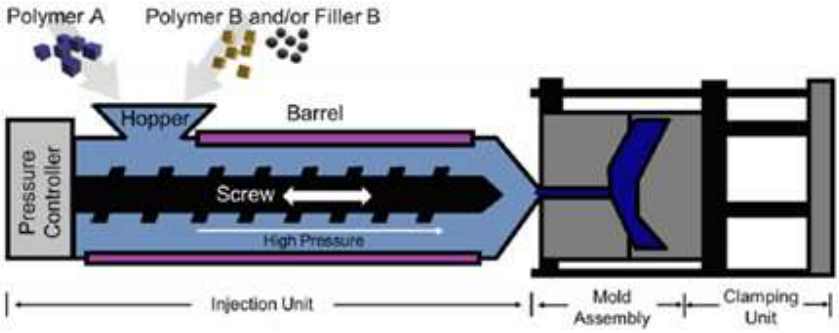

Figure 3. Illustration of melt blending process [18].

The limitation of these methods for the production of polymer composites lies in the fact that they are limited to particular polymers. Solvent blending requires that the polymer be soluble in the solvent for uniform mixing of the reinforcement and polymer to occur. Additionally, the dissolution of the powders in the solvent could introduce contaminants to the composites,

which may not be desired in some applications. On the other hand, melt blending requires that the polymer be melted, which might introduce chemical and structural changes [13].

PEEK has high chemical stability and will not easily dissolve in most organic solvents. Furthermore, it has high thermal stability with a glass transition temperature of 143°C and a melting temperature of 343°C, which is quite high. These properties make it challenging to fabricate PEEK composites using conventional methods [13].

An alternative method that has been investigated in various studies for the production of polymer composites is mechanical alloying. Despite this technique being primarily used in the fabrication of metal composites, it has been successfully used for the production of polymer composites in a number of studies.

3.1.2. PEEK-based composites for tribological applications

PEEK polymer in its pristine form is not ideal to be used as a bearing in implants due to its low wear resistance. For this reason, various studies have been reported, in which attempts have been made to improve the tribological properties of PEEK by reinforcing it with various filler materials.

An example of composite that has proven successful is carbon fibre reinforced PEEK (CFR-PEEK). The incorporation of carbon fibres (CF), which are lightweight, flexible, high-strength and high tensile modulus materials [20], allows increasing the modulus of PEEK to as close to that of the cortical bone (~17GPa) [21]. In fact, carbon fibre reinforced (CFR) polymers are being widely studied as high-performance structural materials in orthopaedic applications due to their low density, high strength and high stiffness [22]. For this reason, many studies opt to use CFR-PEEK instead of pure PEEK for biomedical applications and incorporate additional materials into it that will reduce wear.

Song et al. [23] compared the in vitro wear rate of PEEK and CFR-PEEK against UHMWPE for cervical disk implants. Tribological tests showed a significant difference in the wear rates of PEEK-UHMWPE articulations and those of CFRPEEK-UHMWPE. As can be seen in the tribological results presented in Figure 4, CFR-PEEK-UHMWPE proved to be a better tribo-pair. This was due to the presence of transfer films on the worn surface of CFR-PEEK, which protected the bearing surfaces from wear damage. Furthermore, the carbon fibres restricted the macromolecule of CFR-PEEK from prolapsing easily, thus reducing wear [24].

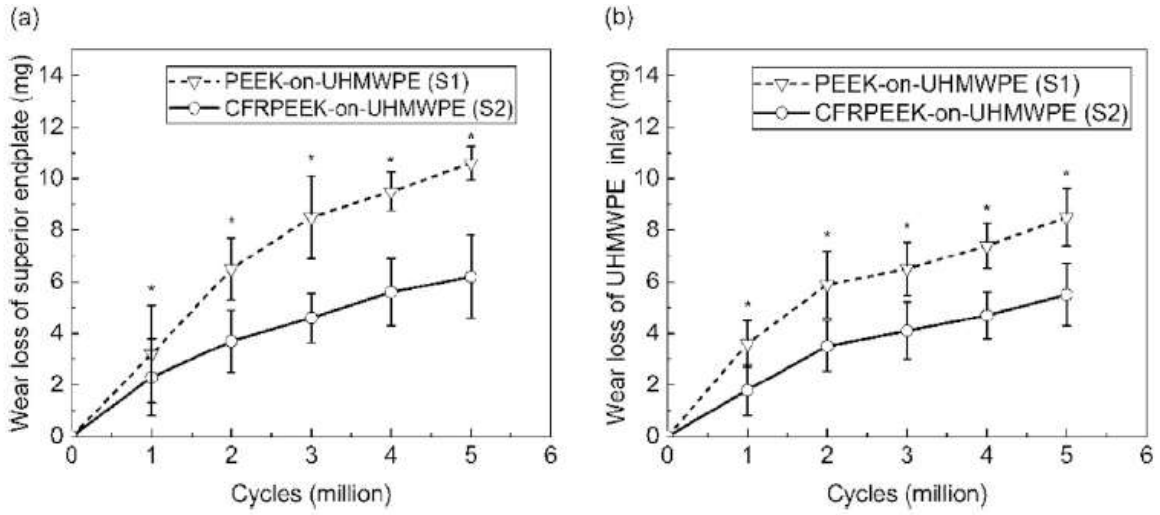

Figure 4. Cumulative mass loss against number of cycles (a) endplate (b) inlay [25].

This study confirmed the benefits of the incorporation of carbon fibres to PEEK. The positive results make the use of reinforced PEEK more promising as a biomaterial. In other studies, pure PEEK has been incorporated with various materials in an attempt to enhance both its mechanical and tribological performance.

Xinke et al. [14] investigated the influence of Molybdenum Disulphide (MS) nanosheets in PEEK for artificial joint applications. Fabrication of MS/PEEK composites (MPC) with contents of 4wt. and 8wt.% was achieved through physical mixing, pressing and sintering. The mixtures were fabricated by magnetically stirring PEEK powders and MS nanosheets in absolute ethanol for 30 min then dried in a vacuum oven at 80°C for 2 h.

The powders were then placed in SS moulds and pressed with a pressure machine at 4 MPa for 2 minutes. They were finally placed in a tube furnace and sintered for 4 hrs in a N_2 atmosphere. It was observed that the addition of MS nanosheets to PEEK increased its wear resistance, more so at a concentration of 8 wt. % (Figure 5-Figure 6). Mechanical properties, i.e., compressive strength and hardness, were also increased as a result. However, an increase of surface roughness with increasing concentration was observed (Figure 7).

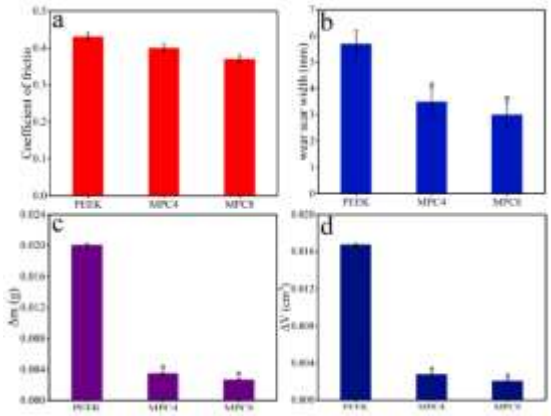

Figure 5. MPC4 and MPC8 after 2 hr of dry sliding [14]: average CoF (a), wear scar width (b), weight wear loss (c), volume wear loss of PEEK (d),

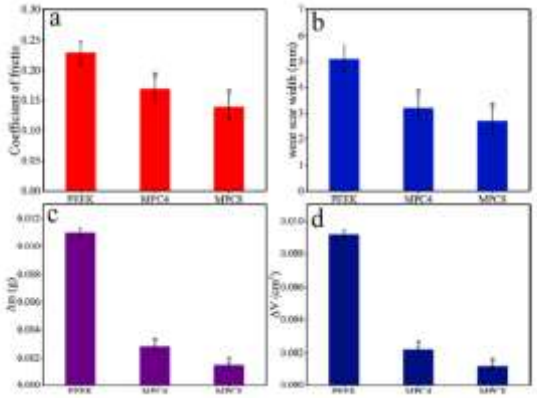

Figure 6. MPC4 and MPC8 after 2 hr of test in water-sliding [14]: average CoF (a), wear scar width (b), weight wear loss (c), volume wear loss of PEEK (d).

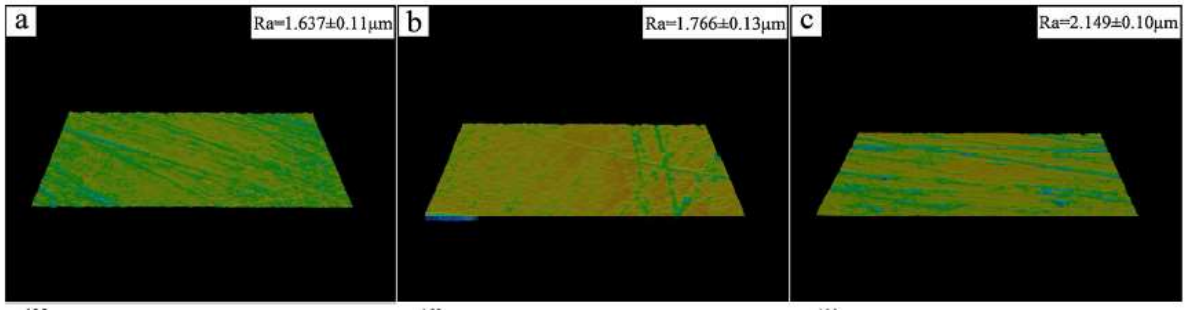

Figure 7. Laser confocal microscope 3D images of PEEK, MPC4 and MPC8 [14].

Puertolas et al. [15] evaluated the mechanical and tribological performance of graphene nanoplatelet (GNP)/PEEK composites.

Graphene nanoplatelets (GNP) are a form of carbonaceous nanomaterial used in a variety of applications due to their high surface area and good self-lubricating property, much like graphite [26]. The characteristic two-dimensional (2D) sheet-like morphology of GNP makes them easier to disperse compared to carbon nanotubes (CNT). Furthermore, GNPs are cheaper and easier to produce than CNTs [26]. The high stiffness, high strength and lubricating capability of GNP were used to enhance the mechanical and tribological properties of PEEK. The nanocomposite was synthesised through melt blending, where the polymer was melted and combined with the desired amounts of GNP. After that, it was extruded through a 2mm diameter die, quenched in a water bath at room temperature, dried and cut into small pellets.

Tensile tests confirmed an increase in mechanical strength and hardness of PEEK with the addition of GNP in the concentrations 3-5wt.%, as seen in Figure 8-9. Tribological tests using a commercial ball-on-disk tribometer revealed the effect of the lubricating capability of GNP on COF. A reduction in the CoF values, as well as wear depth, was observed in the surface profiles, as can be seen in Figure 10-11. However, as the GNP values increased beyond 5wt. %, a decrease in toughness was observed. Furthermore, wear at this stage was observed to

occur through fatigue as opposed to abrasion as in the other cases [15]. Therefore, GNP offered promising results in the enhancement of tribological performance of PEEK as long as its concentration in the mixture was carefully considered.

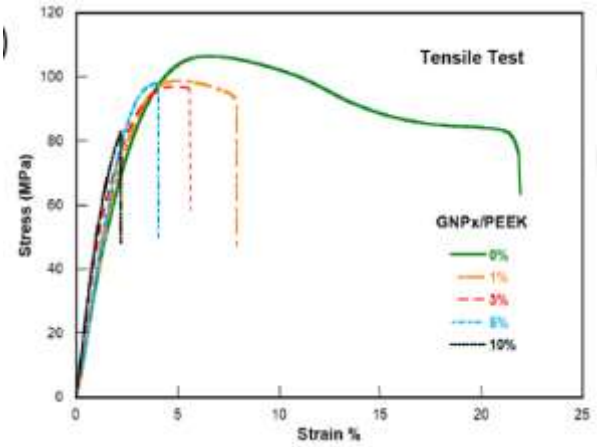

Figure 8. Tensile test of different compositions of GNP/PEEK composites [15].

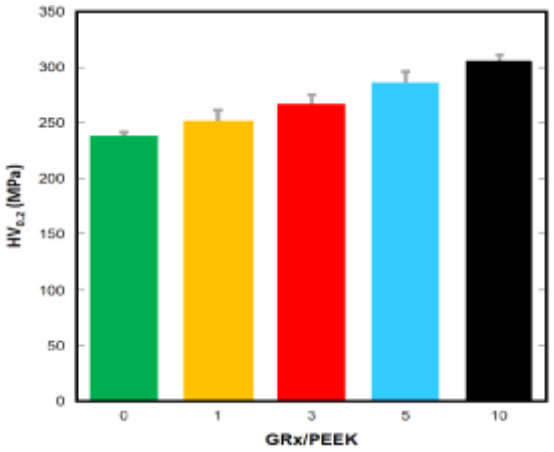

Figure 9. Hardness values of different compositions of GNP/PEEK composites [15].

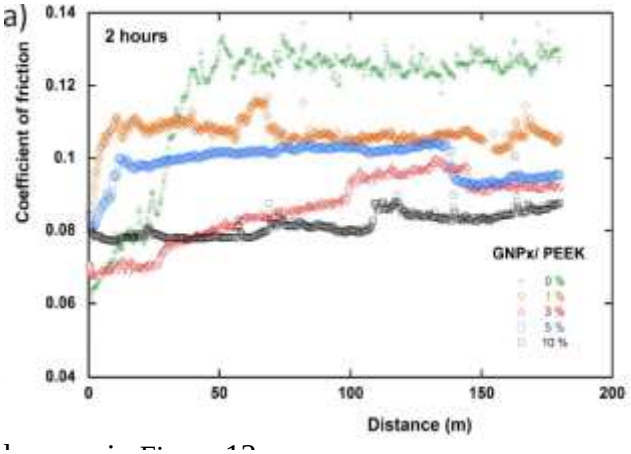

Figure 10. Representation of CoF for different composition of GNP/PEEK composites after 2 hrs of sliding [15]

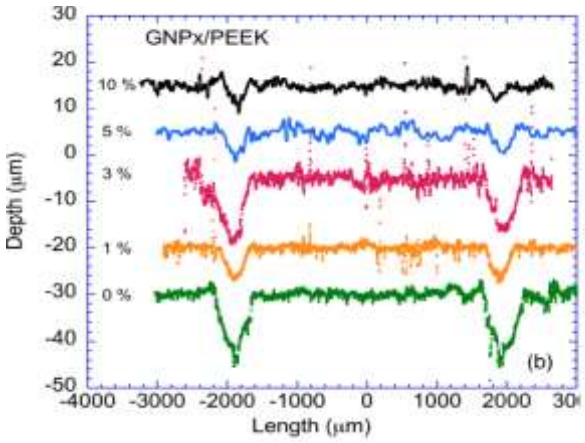

Figure 11. Representation of the surface profile for the different compositions of GNP/PEEK composites after 48 h [15].

Wang et al. [27] experimented on the friction and wear properties of PEEK composite blocks filled with nanometre SiO_2. The composites were formed by dispersing PEEK powder with nanometre SiO_2 then heating under pressure and cooling the mixture. To perform tribological tests, a carbon steel ring was run against the composite block on a block-on-ring machine at various loads. Results revealed that the addition of increasing content of nanometre SiO_2 filler decreased wear rate up to a certain level after which wear rate started to increase again as can be seen in Figure 12.

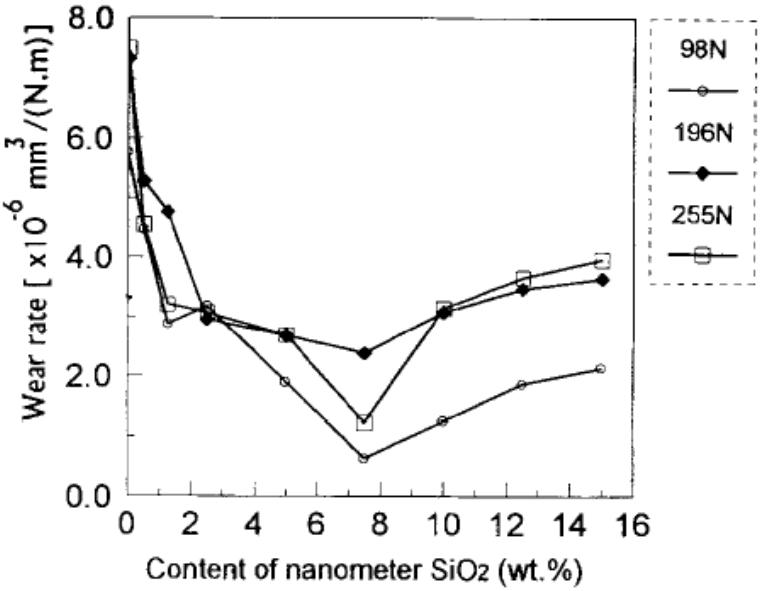

Figure 12. Representation of the WR of PEEK filled with nanometre SiO_2 particles at various loads [27].

Based on the literature, it is clear that the composites reduce CoF and WR through the formation of transfer films/ tribo-layers on the contact areas which serve as solid lubricants that reduce friction.

3.1.3. Mechanical alloying (MA) as an alternative technique to produce PMCs

MA is a unique technique used to produce alloys and compounds that are unable to be produced through conventional methods such as melting [28]. This technique was introduced in the 1960s for the production of oxide-dispersion strengthened nickel alloys. However, its use is no longer limited to the production of metal alloys. Studies have shown that several thermoplastics such as Polystyrene (PS), Polyamide (PA), Polyethylene (PE), PEEK etc. can be processed using this technique. In 1988, Shaw et al. [29] first investigated the use of MA to produce polymeric alloys without the addition of chemical reagents. In this study, PA pellets were mechanically alloyed in a high-energy shaker ball mill at -150°C. It was concluded that the PA particles were refined from large uneven particles to fine layer structure particles after 24h of MA.

3.1.3.1. PEEK-based composites produced by MA

Souza et al.[30], investigated the friction and wear behaviour of two PEEK matrix composites filled with natural amorphous silica fibres (PEEK-NASF) and particulate zirconium-lithium silicate glass fibre (PEEK-LZSA) for dental implant application. The PEEK-based composites were produced by MA of PEEK powder with varying content (10, 20, and 30 mass.%) of either of the fillers at 150 rpm for 24h using zirconia balls. The milled powders were compacted into cylinders by hot pressing at 2 bar then sintered slightly above the melting point of PEEK and held at a pressure of 4 bar for 4 sec. Tribological results from this study did not yield positive

results as there was no improvement in the CoF of the composites when compared to unfilled PEEK as can be seen in Figure 13-Figure 14. In fact, the PEEK-LZSA exhibited increased CoF and higher wear volume compared with unfilled PEEK, while the PEEK-NASF composite had similar results to that of unfilled PEEK.

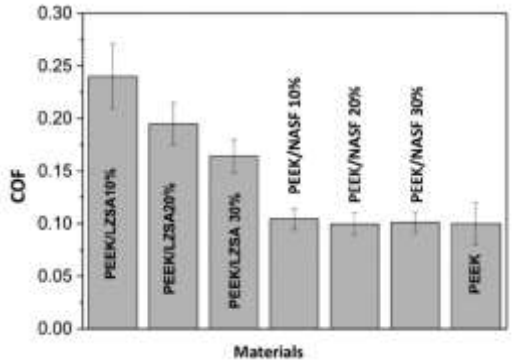

Figure 13. Average steady-state CoF (μ) for PEEK and PEEK-based composites after sliding against alumina in artificial saliva at 37 °C [30].

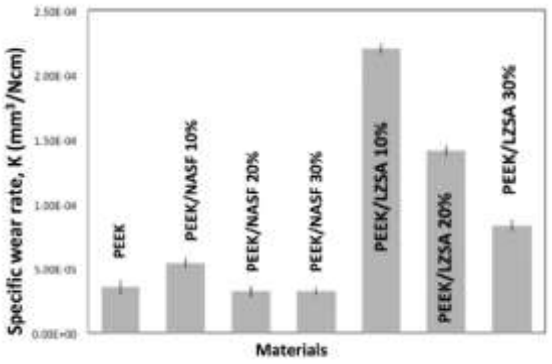

Figure 14. Specific wear rate of unfilled PEEK and PEEK-matrix composites after sliding against (FN = 30 N) alumina in artificial saliva at 37 °C [30].

Javaid et al.[31] investigated the evolution of PEEK's tribological properties by synthesising PEEK-based composites PEEK-MAX (Ti_3SiC_2, Ti_3AlC_2 and Cr_2AlC), and PEEK-MoAlB. The composites were fabricated by ball milling the powder with two PMMA balls, after which they were cold pressed at 175.54 MPa for 30 seconds. The compacted moulds were then hot pressed to 500°C at 117.3 MPa for 5 min then cooled down.

Tribological tests were performed by dry sliding a stainless-steel ball on the composite surfaces. With the addition of Ti_3SiC_2 particulates into the PEEK polymer in increasing amounts, it was observed that the CoF became stabilised compared to that of pristine PEEK, which exhibited erratic behaviour. However, the CoF was not necessarily observed to have decreased. Similar behaviour was observed for the other composites as well as can be seen in Figure 15.

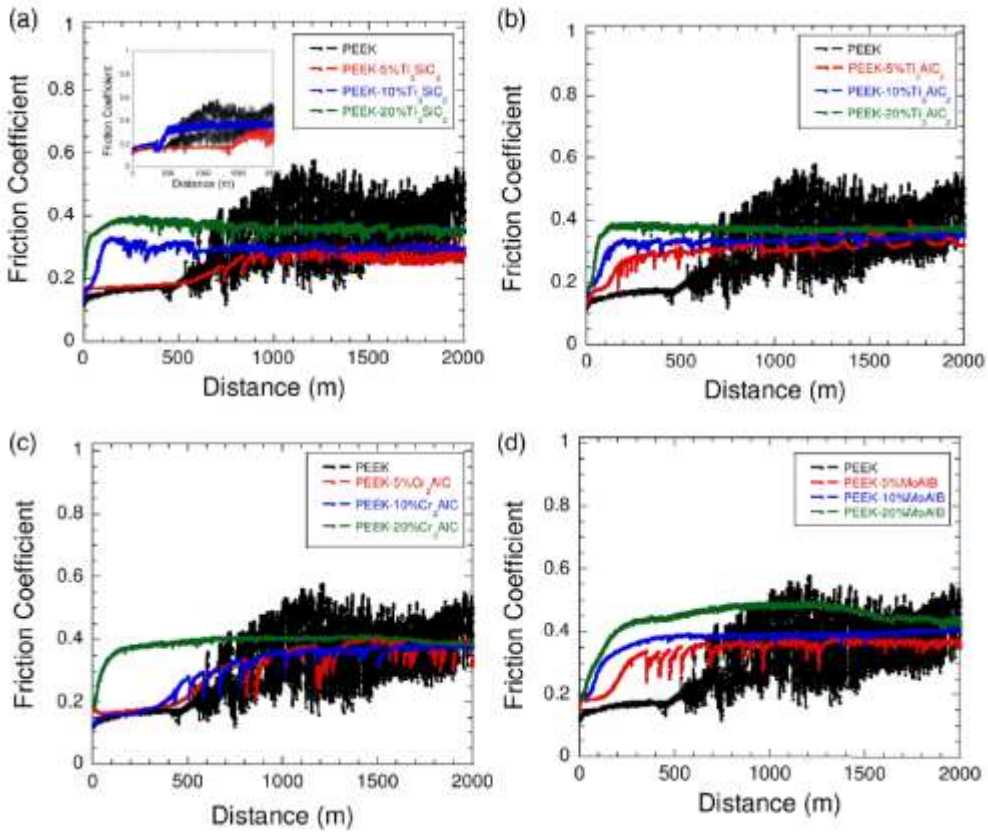

Figure 15. Representation of CoF values as a function of journey distance for: PEEK- Ti_3SiC_2 (inset shows the plot of friction coefficient versus distance of PEEK samples) (a), PEEK- Ti_3AlC_2 (b), PEEK- Cr_2AlC (c), PEEK-MoAlB (d) [31].

Plots of CoF and WR vs MAX (Ti_3SiC_2, Ti_3AlC_2 and Cr_2AlC) or MoAlB content as seen in Figure 16 revealed that the addition of 10 vol.% of MAX or MoAlB resulted in enhanced tribological performance. However, the WR of PEEK- Cr_2AlC was observed to have been higher than others. Tribo-analysis of the surfaces revealed that, the composites worked by forming a triboxide transfer film [31].

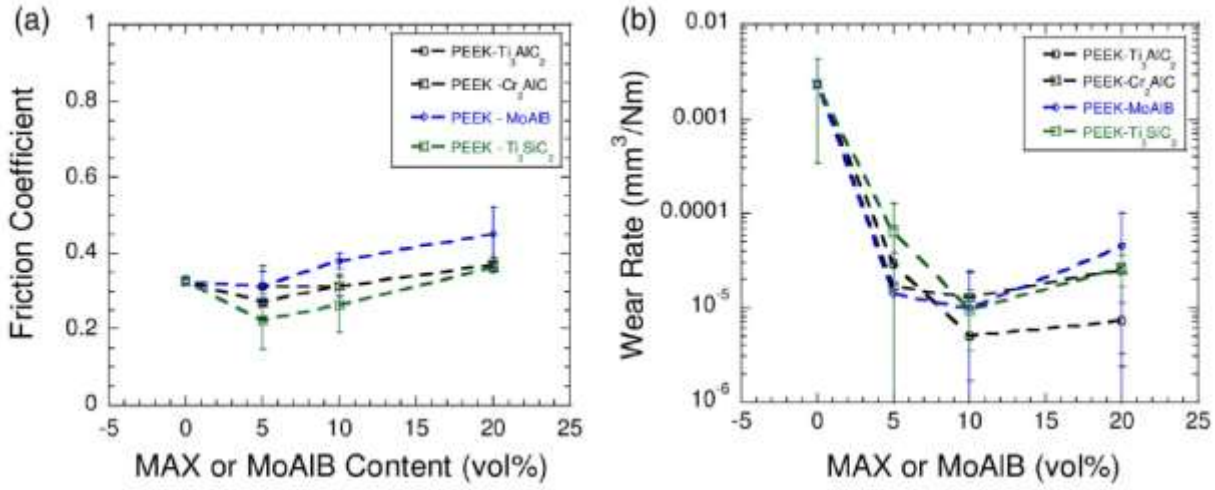

Figure 16. Representation of CoF (a) and WR (b), depending on the content of PEEK-MAX and PEEK-MoAlB composites [31].

From these studies, it can be inferred that the reduction of friction and wear is dependent upon two important factors:

The type of reinforcement
The amount of the reinforcement added to the matrix

The reinforcement in the PMC will act by forming a transfer film on the counter surface which will protect the polymer matrix from abrasion.

In the current research, Sn-Zn-Bi was chosen to act as a soft brazing alloy, while GNP and SCF served as reinforcements. Previous research has demonstrated the biocompatibility of Sn, Zn and Bi metals in the human body.

Gu et al. [32] investigated the cytotoxicity of nine metal elements in the body alloyed with Mg for implant purposes. Sn and Zn were among the metals used to prepare binary alloys with Mg in the concentration Mg-1X (wt.%). It was found that both Sn and Zn improved the strength of Mg and had no toxic effect on the cells. Zn also reduced the corrosion rate of the alloy and had no toxic effect.

Zhen et al. [33] investigated the in vivo biodegradability of a Mg-3Sn-0.5Mn alloy. Results of a haemocompatibility test revealed that the alloy presented superb compatibility to the blood system. Furthermore, Sn served as an age strengthening element to the alloy, which also improved its corrosion resistance [33]. Moreover, Sn ions are rapidly excreted by the kidneys [34].

Zn is an essential trace element in the human body as it is contained in over 300 enzymes and an even larger number of proteins [35]. The availability of Zn is essential in certain bodily functions such as optimal nucleic acid and protein metabolism, cell growth, division and function. Wear particles from orthopaedic implants containing zinc in the body would not have toxic effects, but instead, the Zn^{2+} ions would integrate into the normal metabolic activity. Moreover, Zn^{2+} ions are able to suppress harmful smooth muscle cells and restenosis in arteries while stimulating osteogenesis of the bone [35].

Bi (Bismuth), on the other hand, is a metal with no biological activity. In fact, in its purified form, Bi is used in a number of orally administered pharmaceutical products [34].

In a study by Prasad et al. [36], a Bismuth oxide bioactive glass was developed for the purpose of treating bone-related infections. This bioactive glass was expected to bond to the bone and form an interface that would interact with the physiological environment inside the body. Results of the study confirmed the biocompatibility of Bi^{3+} ions and its antibacterial properties, which could help to prevent chronic bone infection.

The soft brazing alloy together with GNP would work by forming a transfer film and providing constant lubrication, respectively. This way, the surface of the PEEK polymer would be protected during sliding, thus reducing abrasive wear.

4. Materials and methods

The project consists of four tasks: Task 1 and 2 involve the production of the materials, which involves MA of the brazing alloy and reinforcements, followed by the MA of the brazing alloy and reinforcement together with PEEK polymer; while task 3 involves the compaction of the composite powders into moulds at room temperature, and finally task 4 involves characterisation of the materials.

4.1. Raw materials

For the brazing alloy design, elemental Sn (purity 99.9wt.%), Zn (purity 98.8wt.%), and Bi (purity 99.5%) powders from Goodfellow and with average particle sizes of 45, 7.5 and 45 μm, respectively, were used. The reinforcements embedded within the Sn-based brazing alloy consisted of a mixture of short carbon fibres and Graphene nanoplatelets. The SCF, with a filament length and diameter of 80 and 7 μm, respectively, was supplied by Sigrafil, while the GNP (purity 99.9wt.%), with an average thickness and dimensions of 5 nm and dia: 30 μm respectively, was supplied by Nanografi.

4.1.1. Particle size distribution

The average particle size of the blend before milling is presented in Figure 17. A bimodal distribution is observed with two local maxima located at ~10 and ~100 μm. These distributions indicate that there is a wide span between the smallest and largest particle sizes due to the different sizes of the raw materials.

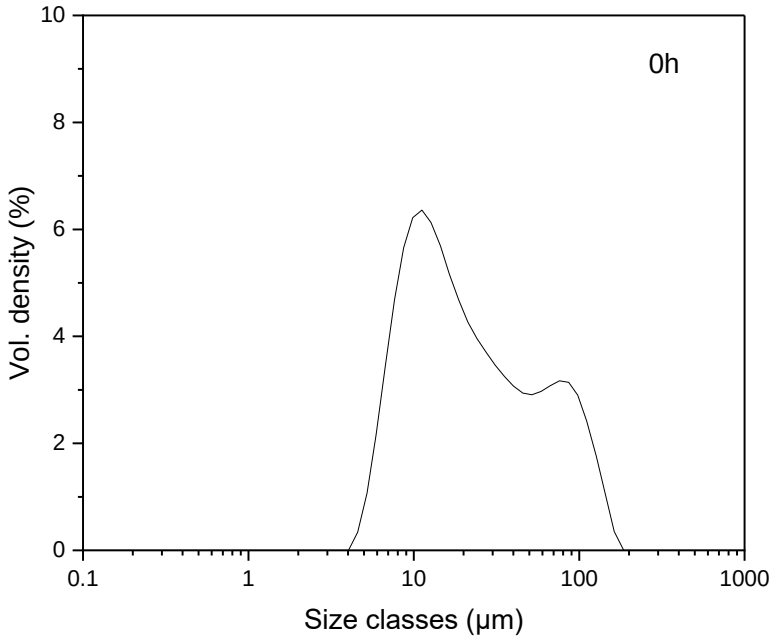

Figure 17. Particle size distribution of the mixtures with 0wt GNP before milling.

4.1.2. Morphology

The images of SEM corresponding to the individual raw powders are presented in Figure 18. The powders of GNP exhibit a flake morphology consisting of stacked layers of graphite sheets, while SCF appear as randomly dispersed cylindrical rods. The powders of Sn have a droplet-shaped spheroidal morphology with a varying size distribution of large and small particles. The powders of Bi have a perfectly round morphology with similar-sized particles. The powders of Zn also exhibit a somewhat spherical morphology with a varying size distribution with some small, medium and large particles. The granulates of PEEK consists of randomly sized particles with no geometrical regularity.

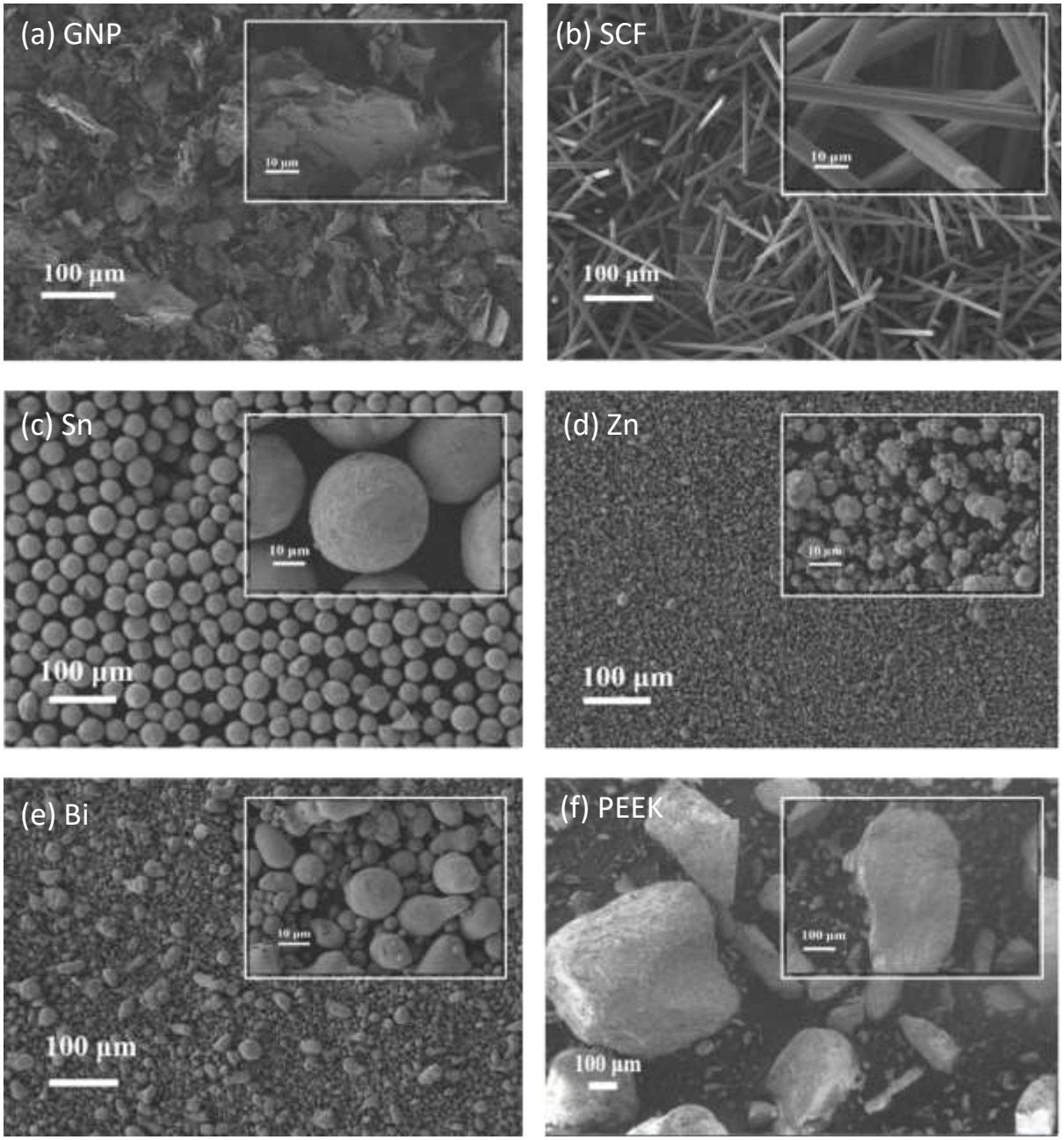

Figure 18. SEM images corresponding to the initial morphology of raw powders: (a) GNP, (b) SCF, (c) Bi, (d) Zn, (e) Sn & (f) PEEK.

4.1.2. Structural evaluation

The crystallographic structure of the raw powders was characterised by XRD, and the results are presented in Figure 19. Strong, sharp diffraction peaks corresponding to the elemental Sn can be seen in the metallic powder blend (Sn-Zn-Bi) due to its high content. Diffraction peaks characteristic of Zn can also be observed. However, due to its very low content in the blend, the diffraction peaks of Bi are barely distinguishable. In addition, pure PEEK granulates exhibit four sharp diffraction peaks at 2Θ ~ 21.5°, 23.7°, 26.0°, 33.0° corresponding to Miller indices 110, 111, 200, 211 of semi-crystalline PEEK [37]. The diffraction pattern of the GNP has one characteristic sharp and intense peak at ~31°, corresponding to the 002 plane. Finally, three wide diffraction peaks at 2Θ ~ 29.5°, 51.1° and 96.2° can be identified as the amorphous structure of SCF.

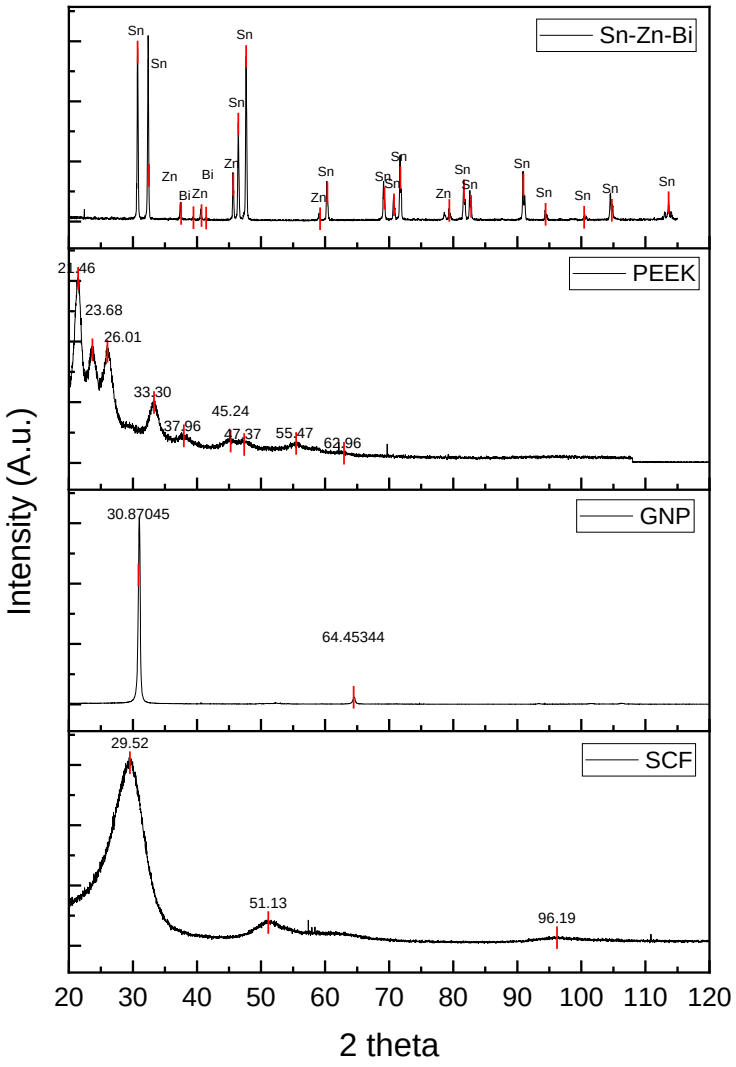

Figure 19. XRD patterns of raw materials.

4.2. Mechanical alloying procedure

Mechanical alloying was selected as a solid-state powder processing route because this method facilitates the repeated welding and fracture of several powder materials with different ductile-brittle nature until the desired microstructure is achieved [38, 39].

The MA process begins with the mixing of powders (with a typical range of sizes from 1 to 500 microns) [38] in given proportions and transferring them to the vial together with the grinding balls. Different alloys can be formed depending on the forms, ranging from metallic powders, intermetallic compounds or dispersoid powders, and character of the components within mixtures, such as ductile-ductile, ductile-brittle or fully brittle metal powders [39].

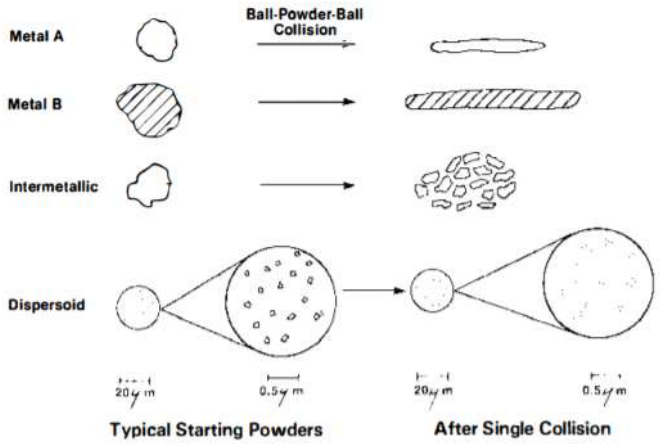

Figure 20. Deformation characteristics of raw powders [38].

Figure 20 presents the effects of a single collision of different types of constituents and how they typically deform [40]. Intermetallic powders fracture and get refined in size, while dispersoids are pulverised severely [40]. However, when the blend is composed of two ductile metals powders (a and b), the milling process becomes more difficult because they are usually flattened and work-harden after a single collision. Moreover, an excess of severe plastic deformation leads to an increased surface-to-volume ratio and causes the films of adsorbed contaminants to rupture. Thereby, when the powder mixture contains a substantial amount of ductile metal, it becomes necessary to introduce a process control agent (PCA). A PCA is an organic compound that acts as a surfactant agent, whereby it adsorbs onto the surface of the metal powders, minimising contact between particles, thus inhibiting their agglomeration. There are many PCAs available, and the choice of PCA depends on the powders being milled. Examples of PCAs include stearic acid, hexane, ethanol, methanol, among others. The disadvantage of PCAs is that they introduce some level of impurities into the metal powder. Therefore, their use should be avoided if a high purity alloy is required [39].

On the other hand, the oxygen content of the metal powders, as well as the nature and amount of impurities, are of importance because these factors influence the final phase of the alloy. Commercial pure metal powders have an oxygen content ranging from 0.05-0.2wt.% [39].

To perform the mechanical alloying of the components, a high energy planetary ball mill (Frisch Pulverisette 7) was selected due to its great versatility to mill ductile and brittle components at high velocities. This type of mill comprises bowls, also known as vials mounted on a rotating disk with a special drive mechanism that causes them to rotate along their axes. The centrifugal forces from the rotating disk around its axis and the autonomous turning of the vials act on the contents of the vial (powders and ball). Since the disk and vial rotate in opposite directions, the centrifugal force is synchronised and opposite [38]. Grinding occurs from the frictional forces between the grinding balls and the vial wall, followed by the high energy impact of the balls and powder as they are lifted off the surface of the vial and collide against the opposite wall at high speed, as shown in Figure 21.

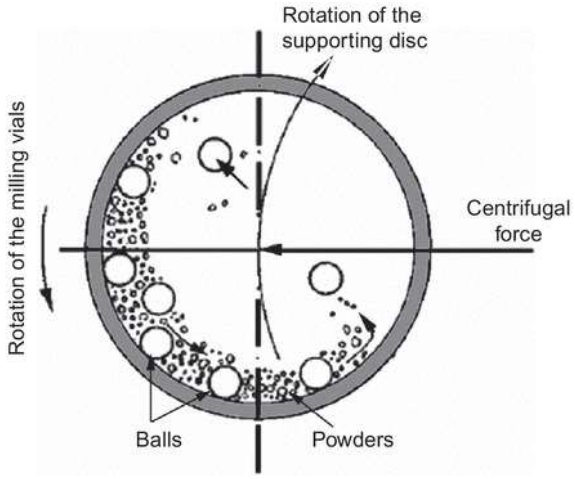

Figure 21. Planetary ball milling mechanism [41].

On the other hand, ball-powder-ball collision modifies the morphology of the metal powder in two ways depending on the type of the constituent particles. Thereby, cold welding takes place when the clean interfaces of the ductile components in the powder overlap, leading to the formation of layered composites. Conversely, the brittle components are normally trapped in the composite and are occluded within the ductile components [38, 40]. As the two processes of cold welding and fracture occur, the layered composites deform into convoluted lamellae, and the microstructure of the powder becomes more refined [40].

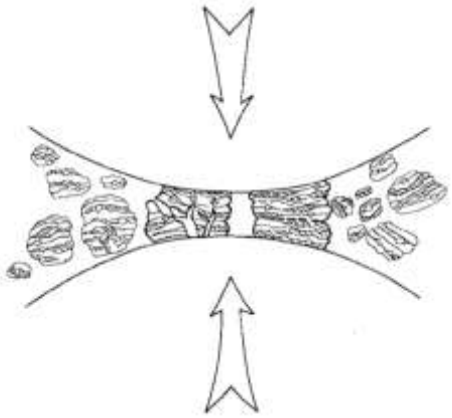

Figure 22. Ball-powder-ball collision of metal powders during MA [40].

As MA continues, the hardness of the powders increases almost linearly with time due to severe plastic deformation. Increasing milling time causes the agglomerated powders to fracture into smaller particles. At the final stage, lamellae are no longer resolvable by optical microscopy, and no further milling can occur [28, 40].

4.2.1. Mechanical alloying of brazing alloy and reinforcements

Four mixtures of powders were prepared in the concentrations of 89wt.% Sn, 8wt.% Zn, 3wt.% Bi, 10wt.% SCF with various GNP contents (0, 3, 7 & 15wt.%) respectively. Besides, 1wt.% of stearic acid was added as a PCA to prevent excessive cold welding of all mixtures. The powder to ball ratio used for milling was 10:1. 30 SS balls were used: 20 with a diameter of 5 mm and 10 with a diameter of 10 mm. A planetary ball mill (Frisch Pulverisette 7) was used for milling, using a speed of 600 rpm and various grinding times. The vials were opened after 1, 3, 5, 10, 15, 20 & 25 h to collect a bit of powder for their characterisation.

4.2.2. Mechanical alloying of PEEK-based polymer matrix composite

Commercial PEEK (085 low density) granulates, supplied by BIEGLO GmbH with an average size of 300 microns, were used across this research. These PEEK granulates were strained to a mean powder size of <250 μm. In total, four composite mixtures composed of 67 wt.% of PEEK and 33 wt.% of reinforcements were made, where the total content of GNP was varied between; 0, 0.99, 2.31 and 4.95wt.%. Following the same strategy as the MA of the brazing alloy plus both reinforcements, the vial was opened after different milling times between 1 and 35 h to collect a bit of powder and thus analyse the particle size evolution of the final mixtures.

4.3. Characterisation

4.3.1. Particle size evolution

Particle size distributions of the blends containing the brazing alloy and reinforcements before and after MA, as well as that of the reinforced PEEK powder after MA, were analysed by a particle size analyser (Mastersizer 30000).

4.3.2. Morphology

SEM (Zeiss Merlin) was used to evaluate the morphology of the blends before and after MA as well as that of the reinforced PEEK powder after MA with the brazing alloy and reinforcements. To improve the conductivity of the PEEK particles for imaging by SEM/EDS, the particles were covered with gold.

4.3.3. Chemical composition and crystalline structure

XRD (Philips XPert) with Co-Ka radiation (λ=1.790300 *A*) was used to analyse the crystalline structure of the powders across different milling times. Moreover, the formation of solid solutions during MA was evaluated across the different milling times.

Mappings of EDS (Oxford Instruments X-MaxN) were performed to evaluate the element distribution and possible presence of segregates within the powders after different milling times.

4.3.4. DSC

Differential Scanning Calorimetry was used to investigate at what point of MA that a single solid solution of the reinforcements was formed. Additionally, DSC was used to determine the change in thermal properties and crystallinity of the PEEK matrix. For that, the different mixtures were subjected to a heating rate of 10°C min^{-1} up to 400ºC.

The degree of crystallinity of the composite powders after compaction was evaluated using the equation

$$X_c(\%) = \frac{\Delta H_f}{\Delta H_{fo}} x100 \ [42] \qquad (1)$$

Where ΔH_f represents the melting enthalpy of the samples and ΔH_{fo} is the standard enthalpy of PEEK normally taken as 130J/g [42].

4.4. Cold compaction procedure

Once the MA of PEEK and fillers (brazing alloy plus both reinforcements) was optimised for the four different conditions of GNP, it was followed by the preparation of several samples by cold compaction. In this compaction route, high-pressure levels are applied at great velocities to consolidate powders. During the increasing pressure, the voids between the particles were reduced, thus reducing the porosity [16].

Sébileau et al.[43] investigated the effect of pressure on the sintering mechanisms of PEEK at low temperature. The hypothesis drawn from their study stated that when particles are under pressure at low temperature (20°C), they undergo rearrangement, which causes friction and induces local heating. This local heating is believed to reach the melting point of the polymer near the surface of the particles allowing higher chain mobility that results in interdiffusion of particles at the interfaces causing cohesion.

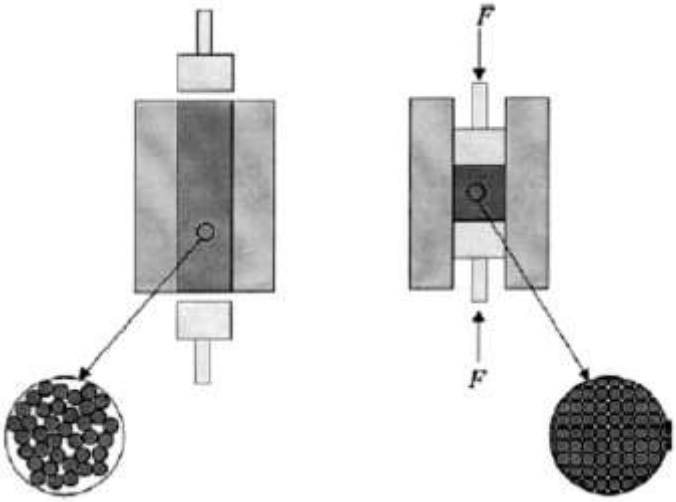

Figure 23. Schematic of compaction process [16].

Five samples in the form of disks (D=26mm, h=3mm) were made by cold compaction. Four of them corresponded with the reinforced PEEK and one with pure PEEK powder. The disks were formed by layering 2g of the MAed reinforced polymer powder on the polished base of the mould then applying some pressure by hand over the powder. Next, an extra layer composed of 2g of the previously strained pure PEEK powder was placed atop the reinforced PEEK layer. The cold compaction was done by applying 40 MPa for 15 min using a hydraulic press.

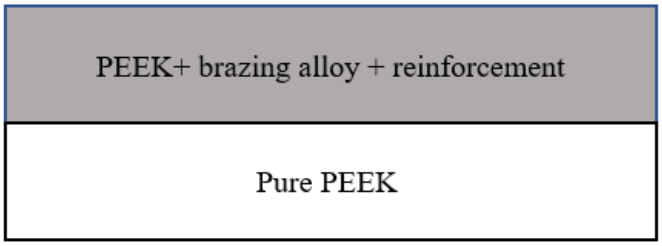

Figure 24. Cross-section corresponding to the PEEK-based polymer matrix reinforced with whiskers of carbon and graphene nanoplatelets embedded in a soft based-Sn brazing alloy on pure PEEK.

The surface of the reinforced PEEK was polished under dry conditions using 1000 & 2400 mesh grit papers, while the bottom surface of the sample was polished with 1000 mesh grit paper to make the base flat. The samples porosity corresponding to the pure PEEK and reinforced PEEK- 3wt. % and 15wt. % samples were characterised using the Autopore IV 9500.

4.5. Mechanical and tribological characterisation

4.5.1. Nanoindentation tests

A Berkovich nanoindenter was used to determine the hardness and Young's Modulus of the samples according to ASTM E 2546. The experiment was carried out at room temperature and using a strain rate of 0.1 s^{-1}.

Hardness was calculated using the equation

$$H = \frac{P_{max}}{A}, A = f h_c^2 \ (f = 24.5), h_c = h - 0.72\left(\frac{P}{S}\right) \ [44] \qquad (2)$$

Where P_{max} denotes the max load applied during indentation, A the projected area of contact between the sample and indenter, s the experimentally measured stiffness and P the load on the indenter.

The Young's modulus was calculated using the equation

$$E = \frac{\sqrt{\pi}}{2}\frac{s}{\sqrt{A}} \ [44] \qquad (3)$$

4.5.2. Pin on disk tests

Before starting the wear characterisation, the samples were glued on commercial PEEK disks, which were previously polished with 1000 mesh grit paper, to give height and stability during the test. Once it was done, wear tests were performed on a unidirectional homemade pin-on-disk tribometer pictured in Figure 25.

Figure 25. Pin on disk tribometer.

A load of 5N was applied through a spherical pin based on a SS (100 Cr^6) ball with a diameter of 10 mm. Before starting, the ball was ultrasonically cleaned in acetone. The rest of the acetone on the surface was removed with ethanol, and after that, the ball was dried into the pin holder.

The radius of the track was set at 7 mm, the total sliding distance in dry conditions was 500 m, and the selected velocity was 0.1 ms^{-1}. The experiment was carried out at room temperature (25°C temperature, 50 % humidity).

A 3D profilometer (Alicona) was used to analyse the wear track and scar on the samples and SS balls, respectively. For the calculation of the wear volume and the specific wear rate of each sample, four profiles across the wear track (on the top, bottom, left and right) were taken. The area and volume of the four points were calculated, and the volume averaged. By means of Origin software, the integration of the removed area across the profiles, measured with the 3D profilometer, were done. The wear volume of the sample and pin were calculated according to ASTM G133. The wear volume of the sample, V_s, was calculated using the equation:

$$V = 2\pi RA, \text{ [45]} \qquad (4)$$

Where R is the radius of the track (7 mm), and A is the average area of the track.

The wear volume, V_b, of the pin was calculated using the equation:

$$V = \frac{\pi h}{6}\left(\frac{3D^2}{4} + h^2\right), \; h = r - \sqrt{r^2 - \frac{D}{4}^2}, \text{ [45]} \qquad (5)$$

Where r represents the radius of the Pin (5 mm) and D the diameter of the scar on the Pin.

The specific wear rate, k, was calculated using the equation:

$$k = \frac{V}{NS}\left(\frac{mm^3}{Nm}\right), [45] \quad (6)$$

Where V_s denotes the wear volume on the sample, N the load applied and S the journey distance.

5. Results and discussion

5.1. Characterisation of MA'ed brazing alloy and reinforcements

5.1.1. Particle size evolution

Figure 26 shows the particle size distribution of the MA'ed blends as a function of GNP content. The evolution of D_{10}, D_{50} and D_{90} values with GNP content and milling times are tabulated in Table 1.

As the MA time increases, the D_{10}, D_{50} and D_{90} values of the three mixtures decrease. Sn, which is the main component of the samples, is a very ductile element, which deforms quite easily during MA. The first stage of deformation occurs inducing deformation, flattening and cold welding as the particles are impacted by the balls. This deformation induces hardening causing the particles to become brittle and tend to break. Therefore, according to the values of Table 1, fracture mechanism predominated from the very beginning of the MA process (1h).

Additionally, with the introduction of 3wt.% GNP into the mixture, a significant reduction in the average size of the particles is seen compared to those at 0wt.%. However, upon increasing the GNP content to 7wt.%, significantly larger particles are observed between 1-5h of MA. This average particle size reduces to more than half its previous size when MA'ed for 15h. In fact, the smallest average particle size is observed in the mixture containing 7wt.% GNP after 25h of MA.

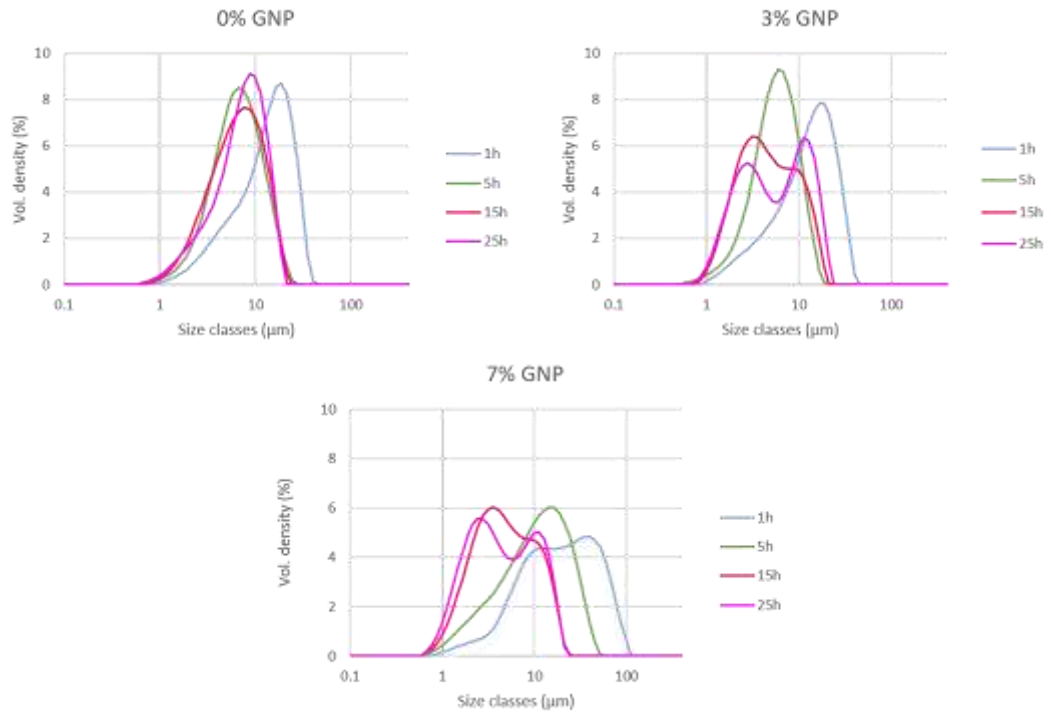

Figure 26. Particle size distribution of the blends: (a) 0 wt.%, (b) 3 wt.%, and (c) 7 wt.% GNP after milling 1, 5, 15, 25 h.

Table 1 Particle size distribution of the blends with 0, 3 and 7 wt.% GNP after milling 1, 15 and 25 h.

GNP content	Time (h)	D_{10} (µm)	D_{50} (µm)	D_{90} (µm)
0%	1	4.32	14.6	27.4
	5	3.01	6.90	14.1
	15	2.70	6.97	14.4
	25	2.75	7.86	14.4
3%	1	3.84	13.9	28.0
	5	2.67	6.03	11.3
	15	1.92	4.67	12.7
	25	1.85	5.66	15.6
7%	1	5.44	20.3	61.7
	5	2.85	11.5	28.6
	15	1.84	4.83	13.7
	25	1.60	4.43	14.1

5.1.2. Morphological and chemical evaluation

The SEM images of the blends after 1h of MA are presented in Figure 27. The corresponding EDS elemental mapping results are presented in Figure 28. After a milling of 1 h, flattened particles can be seen across the blends. Moreover, fragmented SCF rods can still be identified within the mixture as indicated in the Figures.

On the other hand, the EDS mappings show that after a milling of 1h, the powders are not yet homogenously mixed (Figure 28a) because it is possible to see small islands with different contrast embedded within the big particles. These islands will appear brighter or darker depending on the atomic weight of the element. Heavier elements appear brighter. Moreover, Fe and O_2 are detected in the 1h MA'ed mixtures, coming from the contamination of the balls and milling atmosphere, respectively.

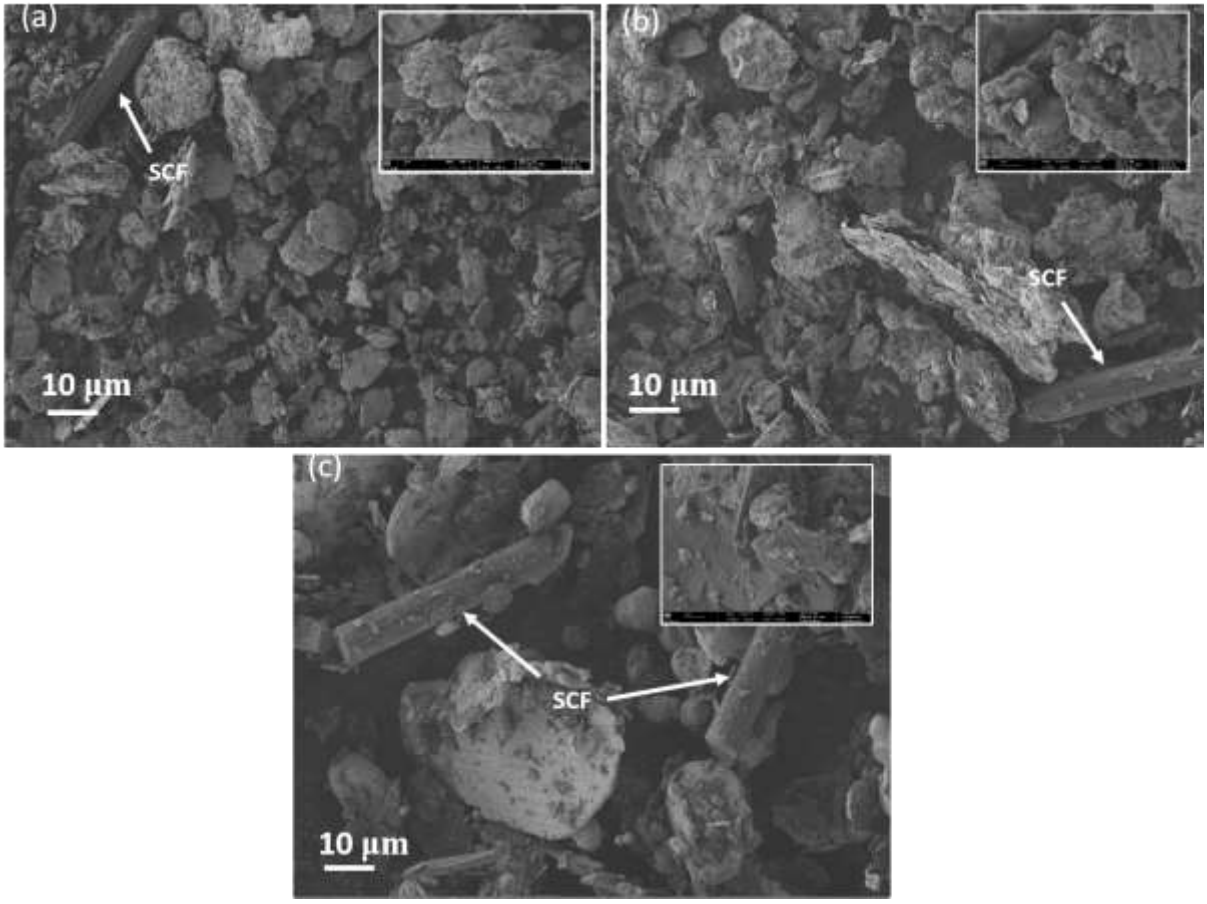

Figure 27. Low and high magnification SEM images of the 1h MA'ed mixtures with different contents of GNP: (a) 0, (b) 3, and (c) 7wt.% GNP, respectively.

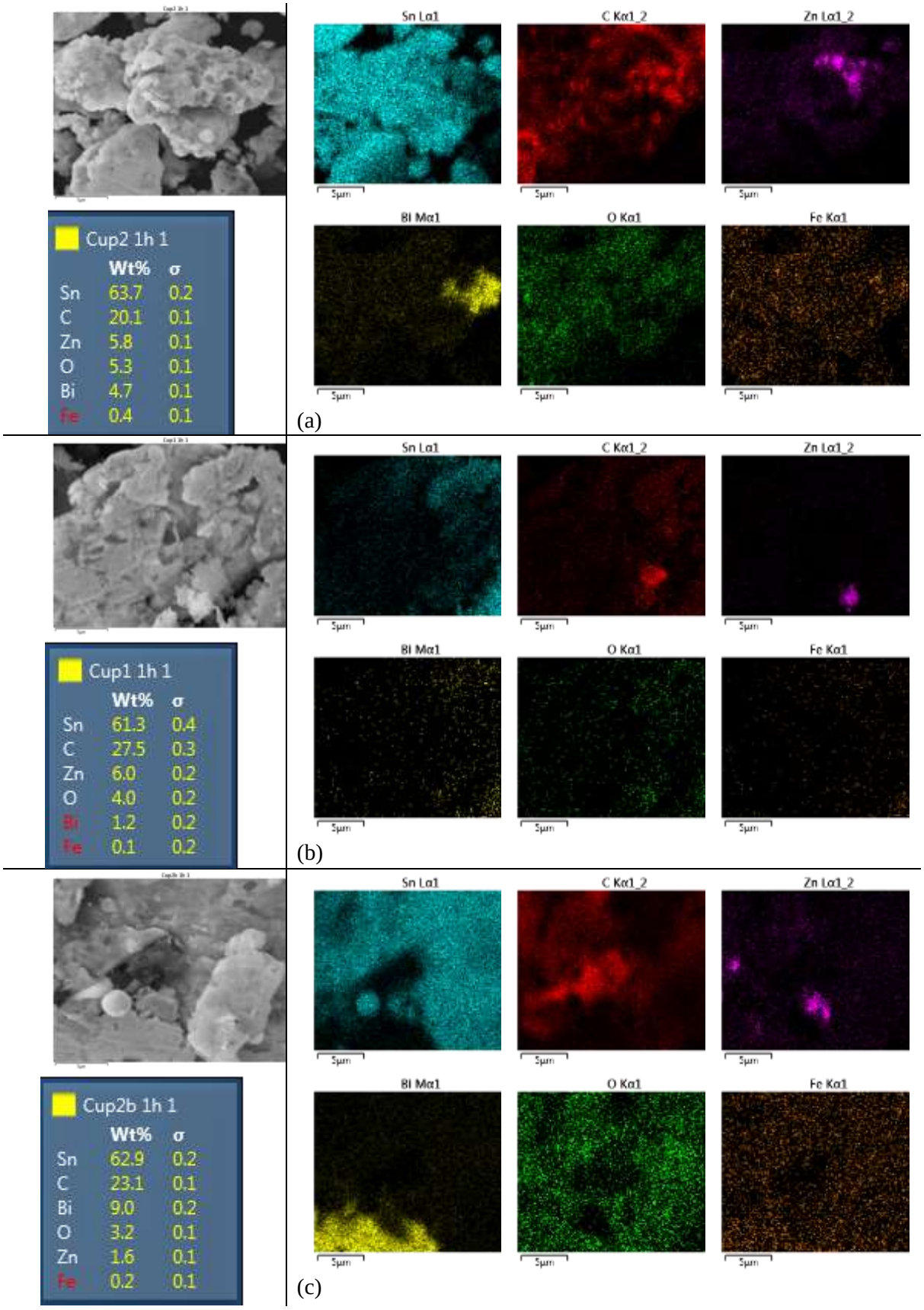

Figure 28. EDS elemental mapping of the 1h MA'ed mixtures with different contents of GNP: (a) 0, (b) 3, and (c) 7wt.% GNP, respectively.

On prolonging the MA time to 15h, the average particle size of the samples is reduced by nearly half (Table 1). At this stage, the powders are work hardened by plastic deformation, which causes them to fracture [46]. Significantly smaller particle sizes are observed in the mixtures containing 3 & 7wt. % GNP compared to the blend with no GNP. This indicates an effect of GNP on the MA process. The incorporation of GNP, which possess high stiffness and high strength, into the ductile blend will foreseeably cause an increase of mechanical properties such as hardness. As a result, the ductility of the blend is reduced, causing fragmentation of the particles to dominate cold welding [15].

The morphology of the powder after a milling of 15h mainly consists of spheroidal agglomerates of the fragmented particles as it can be seen in Figure 29. The blend with no GNP content has the highest D_{50} value (about 7 μm). This confirms that GNP assists in the fragmentation of the particles of the powders.

From the EDS elemental maps after 15h, one might say that the powders are homogenously mixed and negligible segregations are present (Figure 30). At higher milling times, i.e., after 20 and 25 , a bimodal distribution of the particle sizes is observed. This indicates that there is inhomogeneity in the particle sizes. A likely explanation for this is the partial melting at contact points of the powders due to the increase in temperature after long periods of MA, which causes different size particles to form.

For a milling of 25h, no significant morphological changes of the powders was observed. The morphology of the powders is similar to that at 15h, with spheroidal agglomerates of small particles.

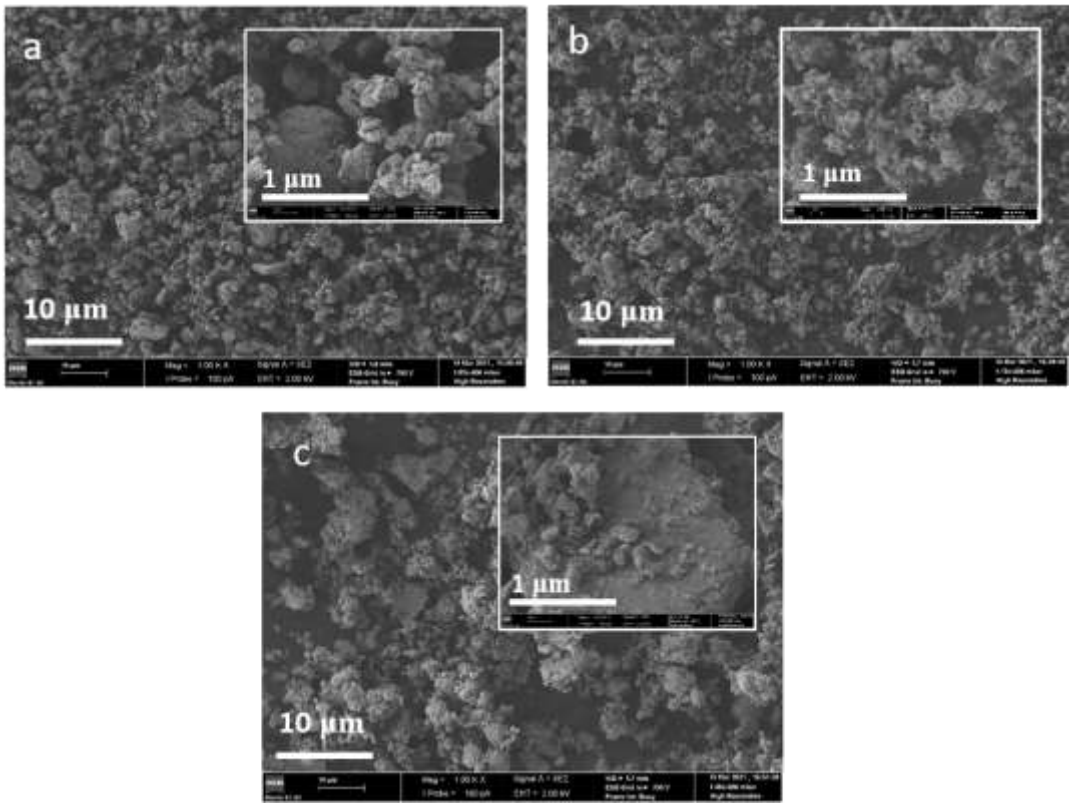

Figure 29. Low and high magnification SEM images of the 15h MA'ed mixtures with different contents of GNP: (a) 0, (b) 3, and (c) 7wt.% GNP, respectively.

15h

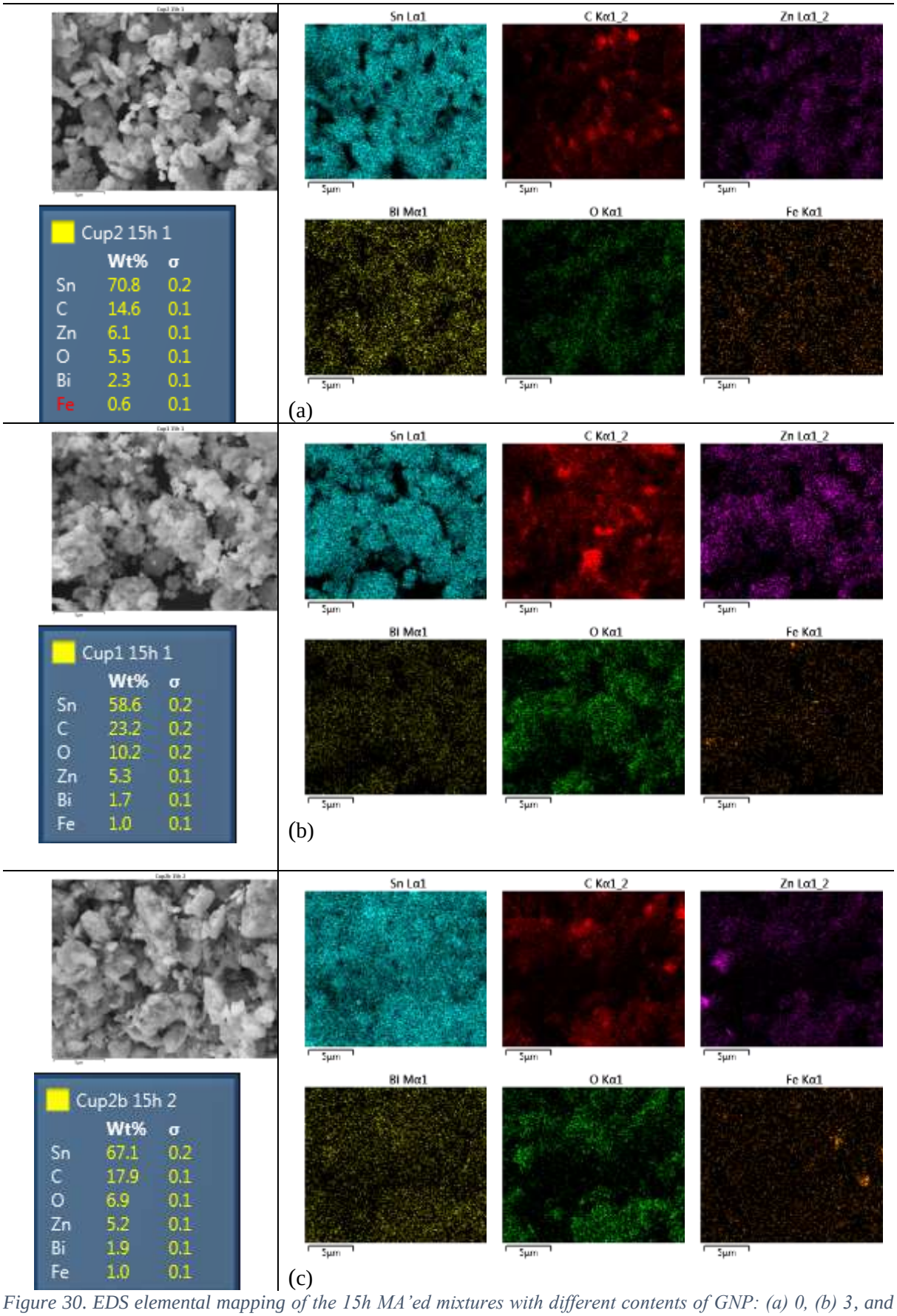

Figure 30. EDS elemental mapping of the 15h MA'ed mixtures with different contents of GNP: (a) 0, (b) 3, and (c) 7wt.% GNP, respectively.

5.1.3. Evolution of the crystal structure

The evolution of the XRD patterns as a function of the GNP content and MA time is presented in Figure 31. For comparison, the position of the peaks corresponding to the constituent metal powders is also shown.

After a MA time of 1h, peaks of the constituent metals, i.e., Sn, Zn and Bi are still detectable. When MA time is increased to 5h, the peaks of Zn and Bi are no longer detectable, which indicates that the dissolution of the atoms of Zn and Bi into the lattice of Sn occurred as observed by Huang et al. [47]. However, no noticeable shift of the Sn diffraction peaks is observed since the atomic radii of these elements are quite similar (1.45, 1.42 and 1.43 A for Sn, Zn and Bi, respectively).

The same case is observed after 15 h of MA. An interesting observation was made for the mixtures containing GNP, where an SnO_2 phase was detected, which did not appear for the mixture with no GNP. A possible explanation for this is the contamination from the environment but it is not clear why this phase was only detectable at these concentrations of GNP.

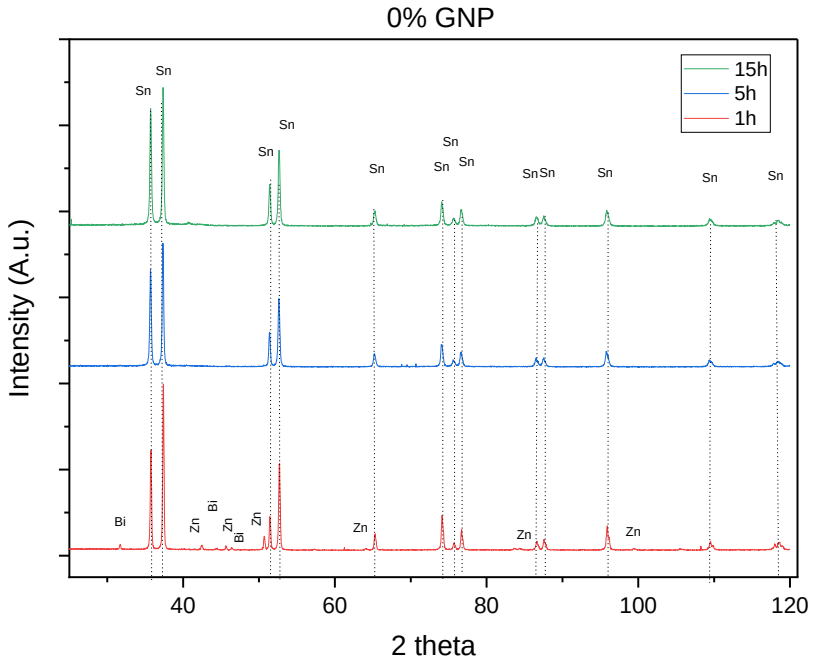

(a)

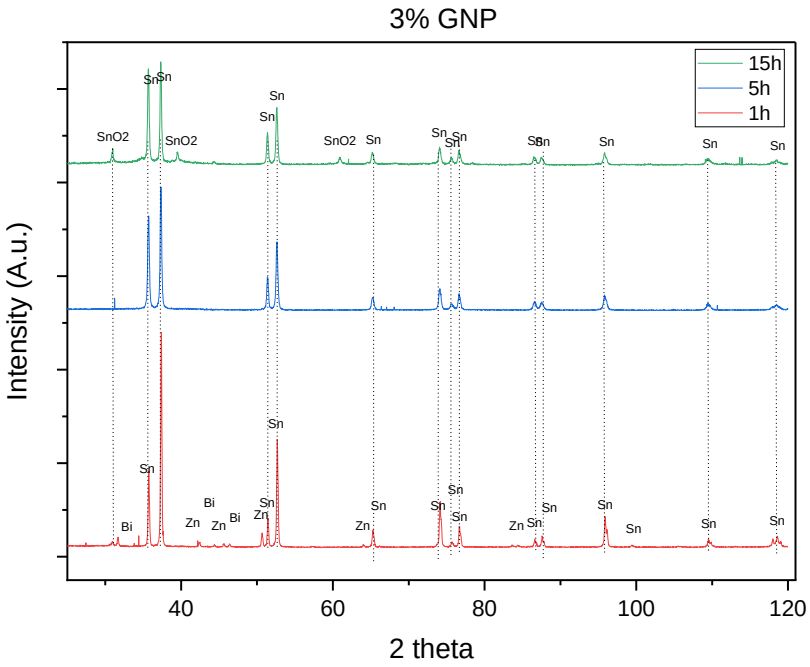

(b)

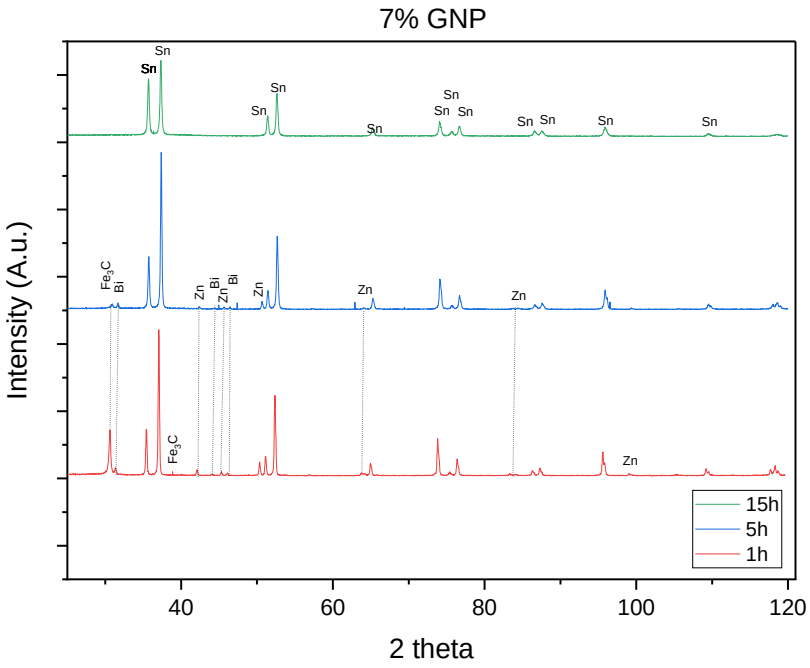

Figure 31. Evolution of XRD diffractograms for all manufactured powder blends as a function of milling time: (a) 0 wt.%, (b) 3 wt.%, (c) 7 wt.%, respectively.

5.1.4. DSC measurements

Figure 32 shows the DSC profiles of the mixture containing 0 wt.% of GNP after MA times of 1, 5 and 15h. After 1 h, an endothermic peak corresponding to the melting of Sn in the Sn-Bi binary phase is observed at around 197°C. At 210°C, an endothermic trough corresponding to the melting of Sn in the Sn-Zn binary phase is seen. This seems to indicate the presence of two Sn rich phases after 1h of MA. The high intensity peak at 232°C corresponds to the melting point of pure Sn, while that at 272°C corresponds to the melting point of pure Bi.

After 5h of MA, only two endothermic troughs are observed which correspond to the melting of Sn in the Sn-Bi binary phase at 196°C and the melting of pure Sn at around 229°C (Figure 33). The troughs are broader and have lower intensity than previous ones. There is also a shift of about (1-2)° of the peaks to the left, which is an indication that alloying is occurring [47].

By 15h, only the endothermic trough of Sn appears with diminished intensity and slightly shifted to the left (Figure 34). This indicates that full alloying has occurred at this stage.

Similar observations are made for the mixture containing 3wt.% and 7wt.% GNP, where the peaks corresponding to the various phases appear after 1h of MA, but disappear by 15h. On top of that the main Sn peak is observed to shift to the left by (1-2)° and to diminish in intensity. This confirmed that a solid solution of the components occurred after 15h of MA.

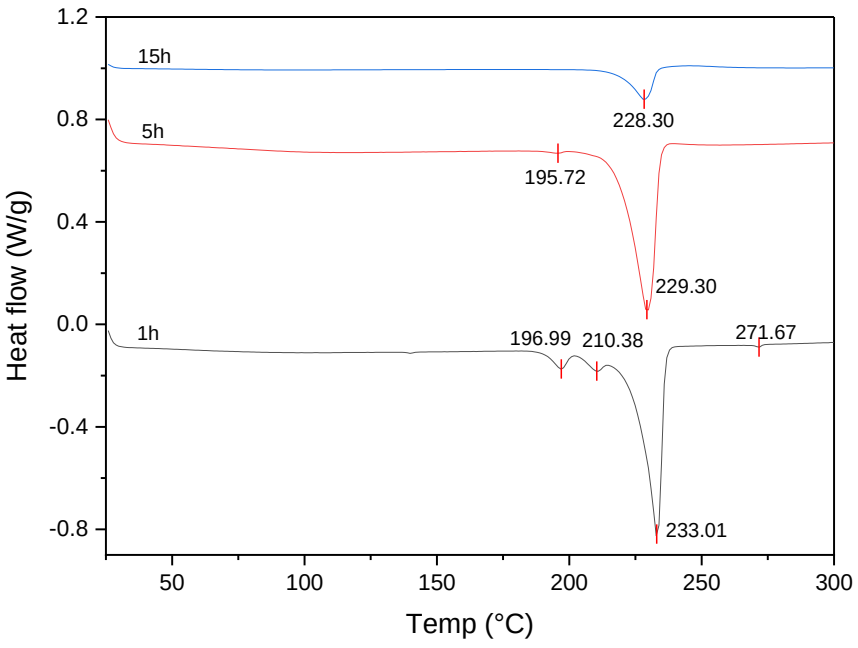

Figure 32. DSC profiles of powder blend containing 0 wt.% GNP MA'ed for 1,5,15 h.

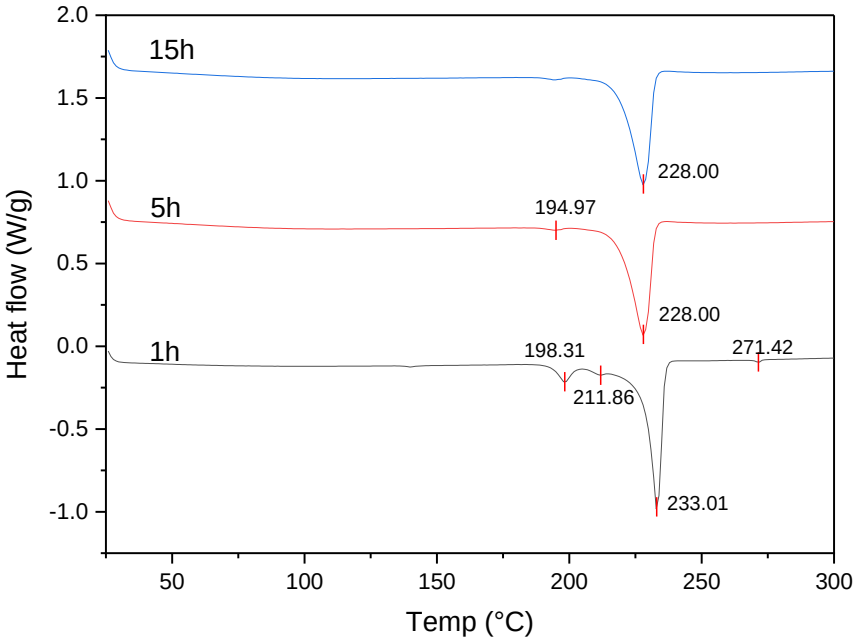

Figure 33. DSC profiles of powder blend containing 3 wt.% GNP MA'ed for 1,5,15h respectively.

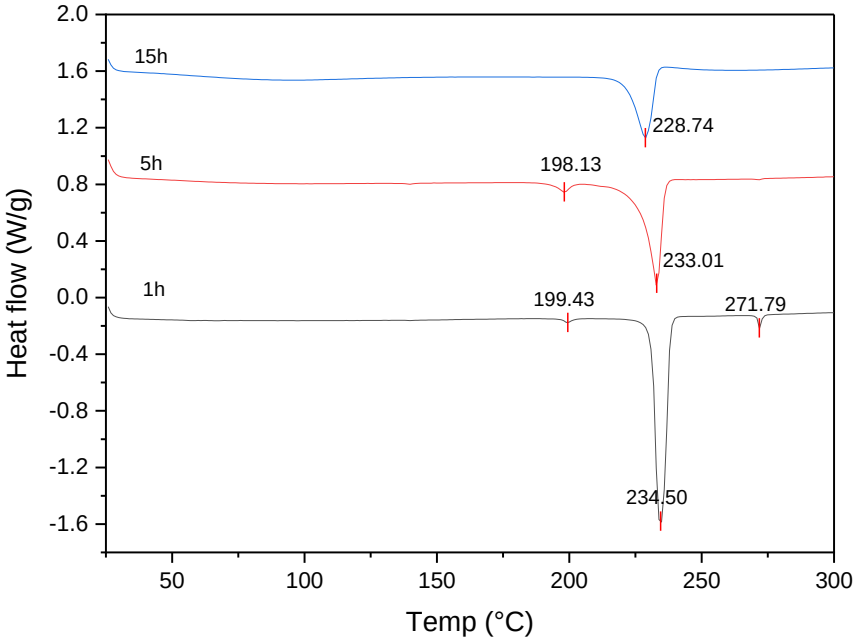

Figure *34. DSC profiles of powder blend containing 7 wt.% GNP MA'ed for 1,5,15h respectively.*

5.2. Characterisation of reinforced based-PEEK matrix polymer

5.2.1. Particle size evolution

Four composite mixtures composed of 67 wt.% of PEEK and 33 wt.% of reinforcements were made, where the content of SCF was fixed to 3.3 wt.% while the content of GNP was varied between 0, 0.99, 2.31 and 4.95 wt.%.

Figure 35 presents the optimised particle sizes for the reinforced based-PEEK powders blends containing 0, 0.99, 2.31 and 4.95 wt.% after milling times of 20, 18, 15 and 35h, respectively. The powders were MA'ed until they obtained similar sized particles. The corresponding D_{10}, D_{50} and D_{90} values are tabulated in Table 2.

As it can be seen, the smallest average particle size measuring ~15 μm is observed in the composites containing 2.31wt.% and 4.95wt.% GNP. The largest average particle size is observed in the composite containing no GNP. This confirms the effect of GNP in enhancing the fragmentation of particles during the MA process even when they are MA'ed and alloyed with soft and ductile material as PEEK polymer. Smaller particles are more desirable for the cold sintering process because they result in higher densification [48].

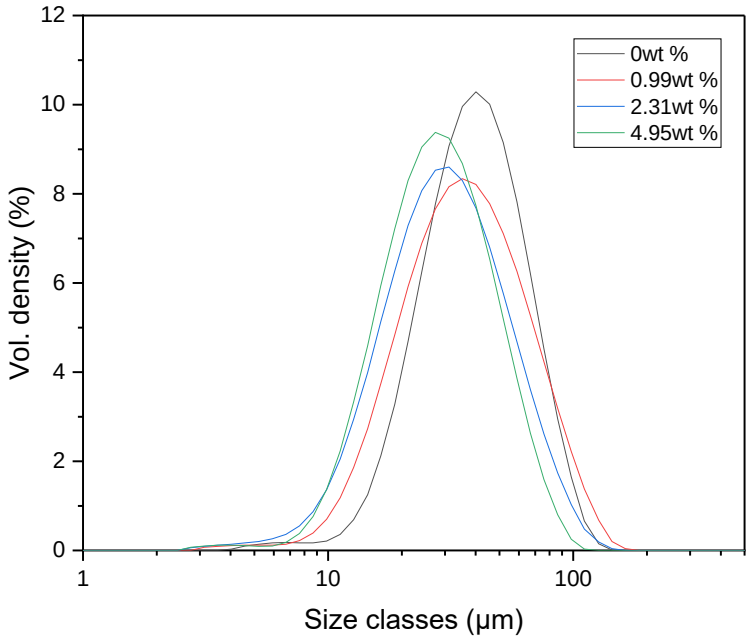

Figure 35. Agglomerate size distribution of reinforced based-PEEK powder blends containing 0, 0.99, 2.31, 4.95 wt.% GNP after milling times of 20, 18, 15 & 35h, respectively.

Table 2. Particle size distribution of the reinforced based-PEEK powder blends with 0, 0.99, 2.31 and 4.95wt.% GNP after milling.

GNP (wt.%)	Time (h)	D_{10} (µm)	D_{50} (µm)	D_{90} (µm)
0	20	21.9	41.9	75.9
0.99	18	17.7	38.1	80.6
2.31	15	14.8	31.8	66.3
4.95	35	14.9	29.7	57.7

5.2.2. Morphological evolution

The images of SEM corresponding to the reinforced based-PEEK powder blends containing 0, 0.99, 2.31 and 4.95wt.% GNP after MA times of 20, 18, 15 & 35h, respectively, are presented in Figure 36. Although milling times are quite dissimilar, the final average particle size is comparable for all of them. As it can be seen, the general morphology of the MA'ed composite powders blends consists of flakes. The largest average particle sizes (~42μm) are observed in the blend containing 0 wt.% GNP. As the content of GNP is increased, the average particle size descends slightly with no apparent direct relationship to MA time.

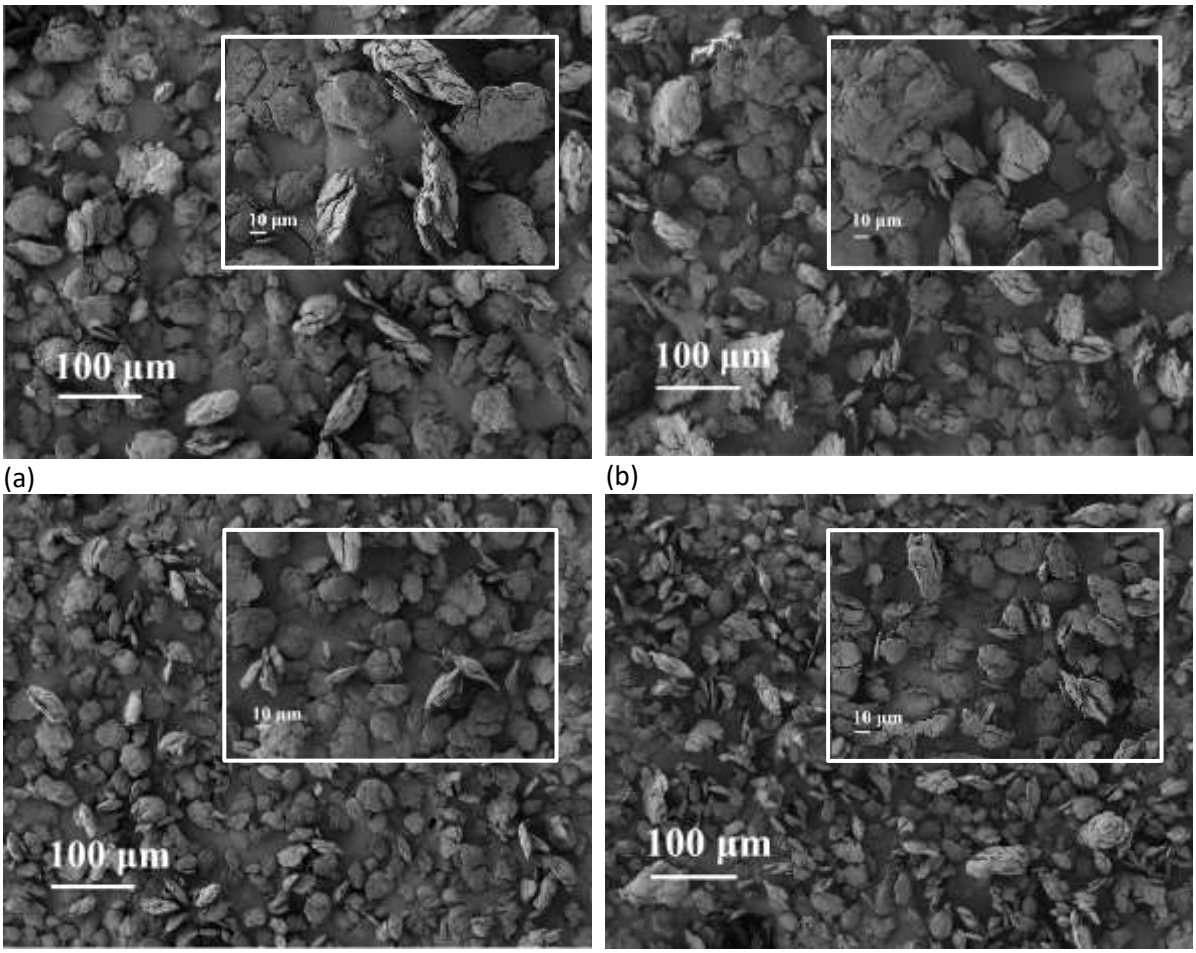

Figure 36. Images of SEM corresponding to the reinforced based-PEEK powder blends composites containing (a) 0, (b) 0.99, (c) 2.31, (d) 4.95 wt.% GNP after milling times of 20, 18, 15 & 35h, respectively.

The mappings of EDS corresponding to these reinforced based-PEEK powder blends are presented in Figure 37. As it can be seen, there is a homogenous distribution of particles corresponding to whiskers of carbon and the Sn-based brazing alloy within the agglomerates of PEEK in the form of flakes. This flake morphology is quite common when ductile polymers, as PEEK, are subjected to high energy mechanical alloying during long milling times.

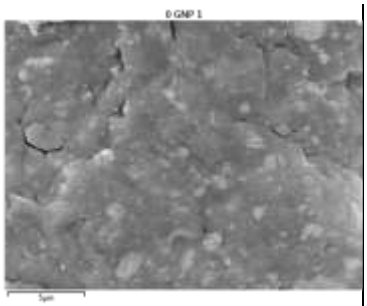

0 GNP 1	Wt%	σ
C	62.0	0.2
Sn	20.5	0.1
O	14.1	0.1
Zn	2.2	0.0
Bi	0.8	0.1
Fe	0.3	0.2

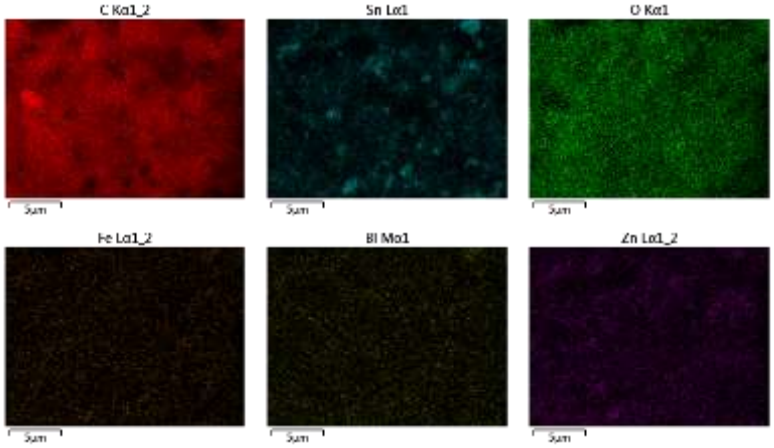

(a)

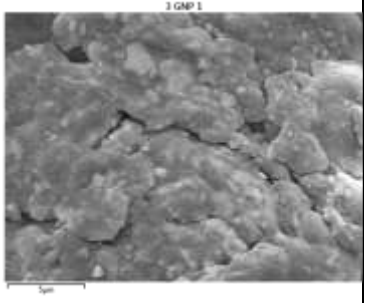

3 GNP 1	Wt%	σ
C	62.3	0.1
Sn	20.1	0.1
O	14.2	0.1
Zn	2.2	0.0
Bi	0.7	0.1
Fe	0.3	0.1

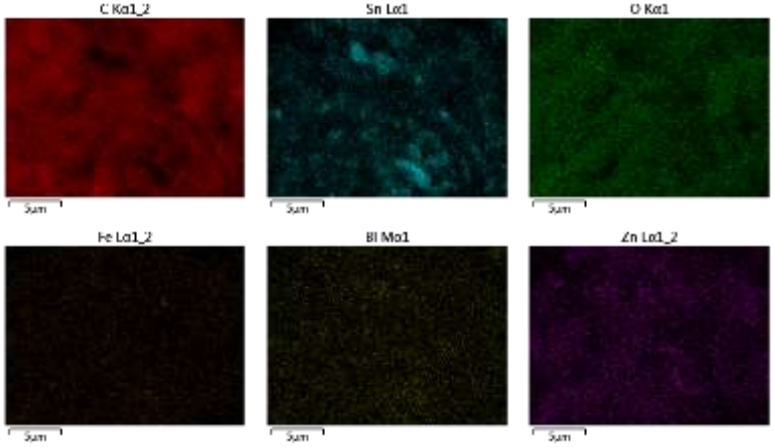

(b)

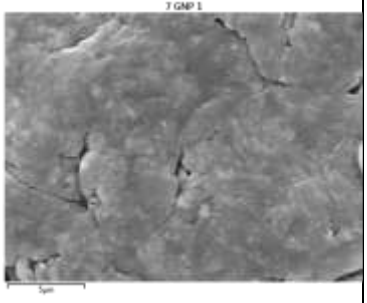

7 GNP 1	Wt%	σ
C	62.7	0.2
Sn	18.8	0.1
O	15.2	0.1
Zn	1.9	0.0
Bi	0.8	0.1
Fe	0.6	0.2

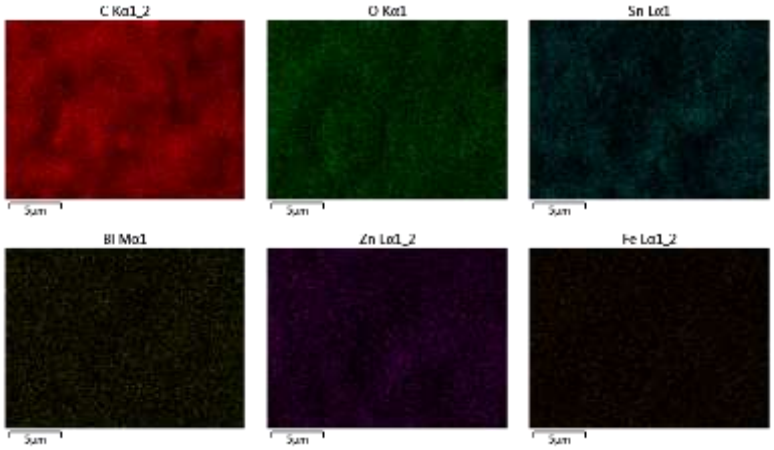

(c)

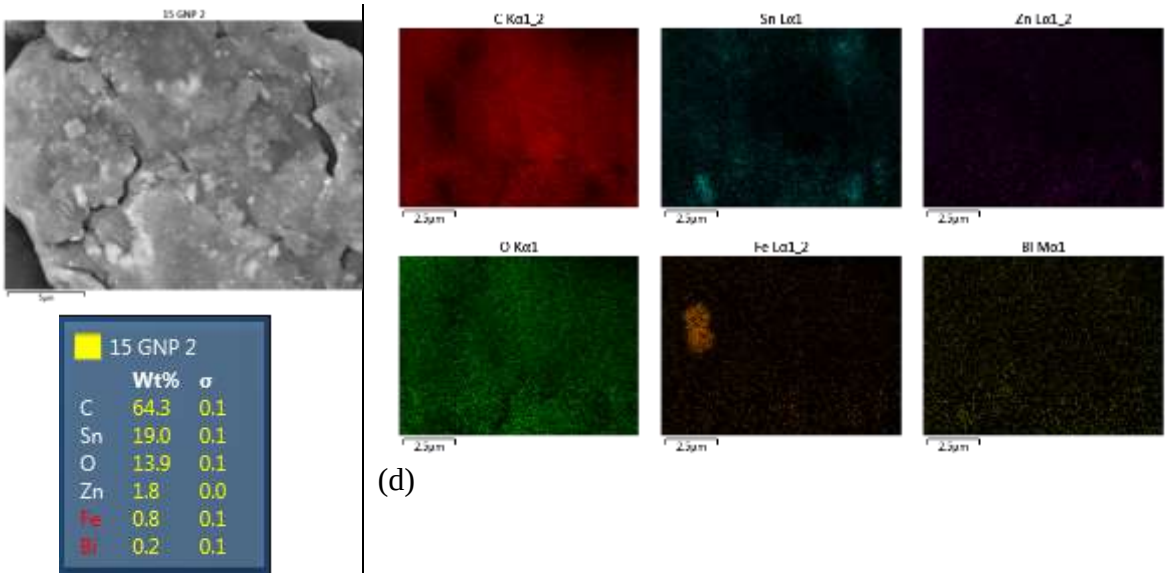

(d)

Figure 37. Elemental EDS mappings performed on the reinforced based- PEEK powder blends containing (a) 0, (b) 0.99, (c) 2.31, and (d) 4.95wt.% GNP after milling times of 20, 18, 15 & 35h, respectively.

5.2.3. DSC measurements

Results of the DSC measurements corresponding to the reinforced based-PEEK powders blends are presented in Figure 38 and Table 4. This technique was used to study the effect of MA and the presence of both reinforcements embedded in the based-Sn brazing alloy on the melting (T_m) and crystallisation temperatures (T_c) of PEEK, as well as how its degree of crystallinity changes.

As it can be seen from all the heating curves, three peaks are observable at 150±2 °C , 224±2 °C and 351±2 °C These peaks correspond to the cold crystallisation (T_{cc}) of PEEK, the T_m of the solid solution of Sn and the T_m of the PEEK powder, respectively. With the addition of increasing concentration of GNP, there is no significant shift observed in the T_m and T_{cc} of PEEK. However, there is a significant difference in the heat of cold crystallisation as can be seen in Table 4. The ΔH_{cc} is seen to increase from (6.49, 8.225, 8.238) J/g in the presence of (0, 0.99, 2.31)wt.% GNP but reduces to 6.288 J/g for 4.95wt.% GNP. The larger ΔH_{cc} values can be attributed to the local amorphisation induced in the structures as a result of MA. The lower ΔH_{cc} seen in the composite containing 4.95wt.% cannot be directly explained because this mixture was MA'ed for a significantly longer duration than the others.

The cold crystallisation peak of PEEK is observed at 288.2°C, 289.9°C, 290.1°C and 264.1°C for the composites containing 0, 0.99, 2.31, 4.95wt.% GNP respectively. The shift of this peak for the composite powder blend containing 4.95 wt.% of GNP indicates a significant change in the crystallinity of the reinforced PEEK. The reason for this is that MA causes the deterioration of PEEK crystallites thus decreasing the degree of crystallinity [13]. Furthermore, the increasing concentration of GNP in the polymer matrix causes a reduction in the mobility of chain segments of PEEK thus reducing the crystallinity. Similar results were observed by Hedayati et al. [13]

Another interesting observation can be made in the cooling curves of the composites containing 2.31 and 4.95wt.% GNP, where the peak at ~140°C disappears. Only the peak corresponding to the crystallisation of PEEK appears. This could indicate that a solid solution is formed from the reinforcements and PEEK powder.

The degree of crystallinity (X_c) was calculated using the equation

$$X_c(\%) = \frac{\Delta H_f}{\Delta H_{fo}} x100 \text{ [42]} \qquad (7)$$

Where ΔH_f represents the melting enthalpy of the samples and ΔH_{fo} is the standard enthalpy of PEEK taken as 130J/g. The results of the degree of crystallinity are presented in Table 3.

As it can be observed, the degree of crystallinity slightly increases when 0.99 wt.% of GNP is added to the mixture. The degree of crystallinity of the samples containing 0, 0.99, 2.31wt.% are quite close in value and no significant change in crystallinity occurs. However, when the GNP content is increased to 4.95wt.%, the degree of crystallinity decreases.

Table 3 Crystallinity calculation of PEEK composites containing 0, 0.99, 2.31, 4.95wt.% GNP

Sample	**0 wt.%**	**0.99 wt.%**	**2.31 wt.%**	**4.95 wt.%**
X_c (%)	32.58	32.75	32.53	28.38

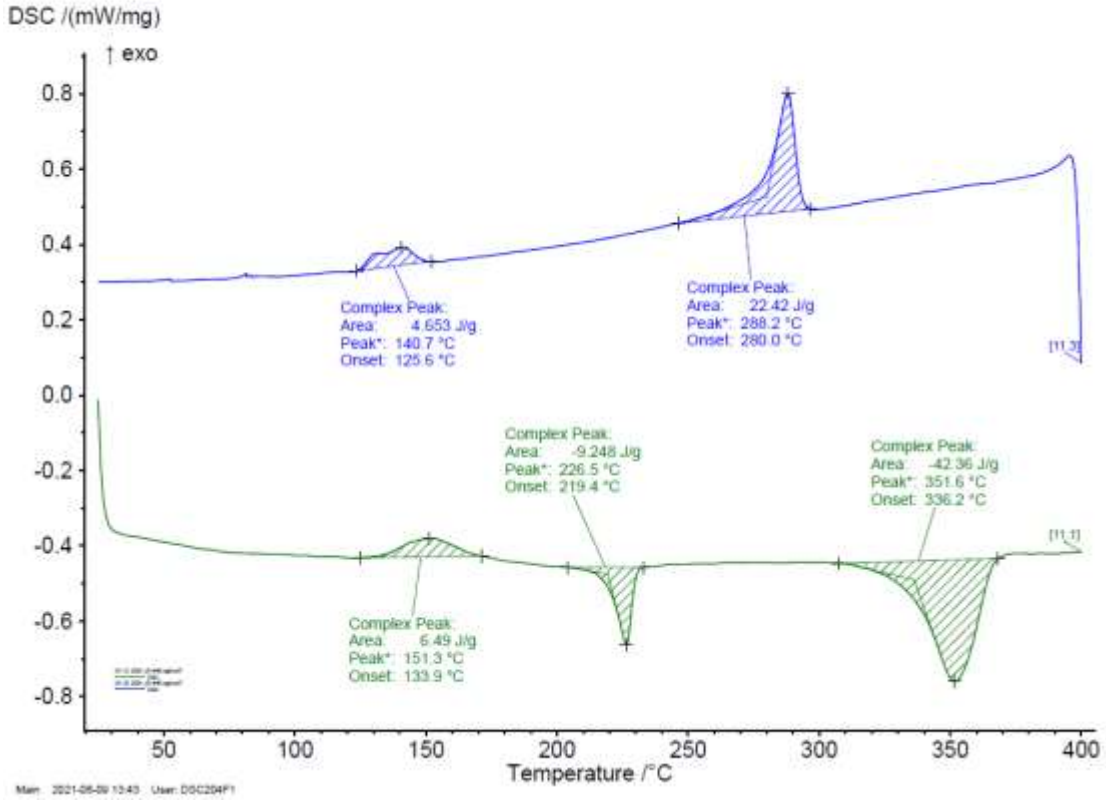
DSC /(mW/mg)
↑ exo
0.8
0.6
0.4
0.2
0.0
-0.2
-0.4
-0.6
-0.8
Complex Peak:
Area: 4.653 J/g
Peak*: 140.7 °C
Onset: 125.6 °C
Complex Peak:
Area: 22.42 J/g
Peak*: 288.2 °C
Onset: 280.0 °C
Complex Peak:
Area: -9.248 J/g
Peak*: 226.5 °C
Onset: 219.4 °C
Complex Peak:
Area: -42.36 J/g
Peak*: 351.6 °C
Onset: 336.2 °C
Complex Peak:
Area: 6.49 J/g
Peak*: 151.3 °C
Onset: 133.9 °C
50
100
150
200
250
300
350
400
Temperature /°C

(a)

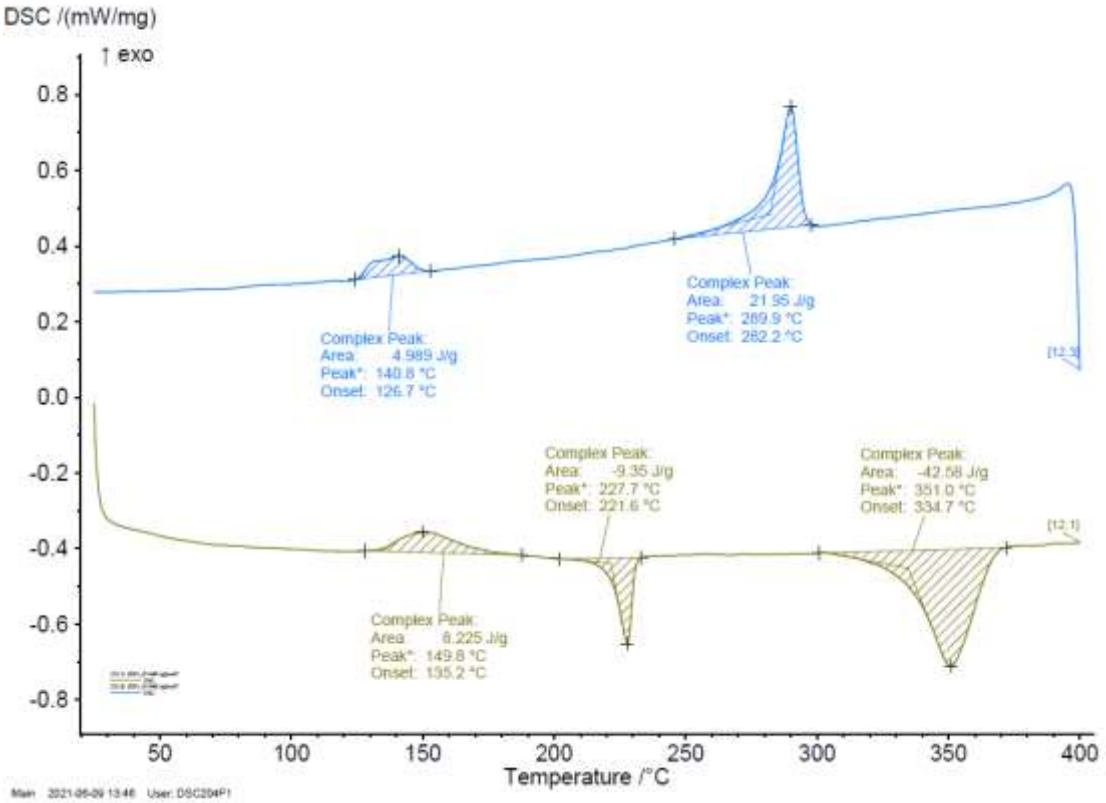
DSC /(mW/mg)
↑ exo
0.8
0.6
0.4
0.2
0.0
-0.2
-0.4
-0.6
-0.8
Complex Peak:
Area: 4.989 J/g
Peak*: 140.8 °C
Onset: 126.7 °C
Complex Peak:
Area: 21.95 J/g
Peak*: 289.9 °C
Onset: 282.2 °C
Complex Peak:
Area: -9.35 J/g
Peak*: 227.7 °C
Onset: 221.6 °C
Complex Peak:
Area: -42.58 J/g
Peak*: 351.0 °C
Onset: 334.7 °C
Complex Peak:
Area: 8.225 J/g
Peak*: 149.8 °C
Onset: 135.2 °C
50
100
150
200
250
300
350
400
Temperature /°C

(b)

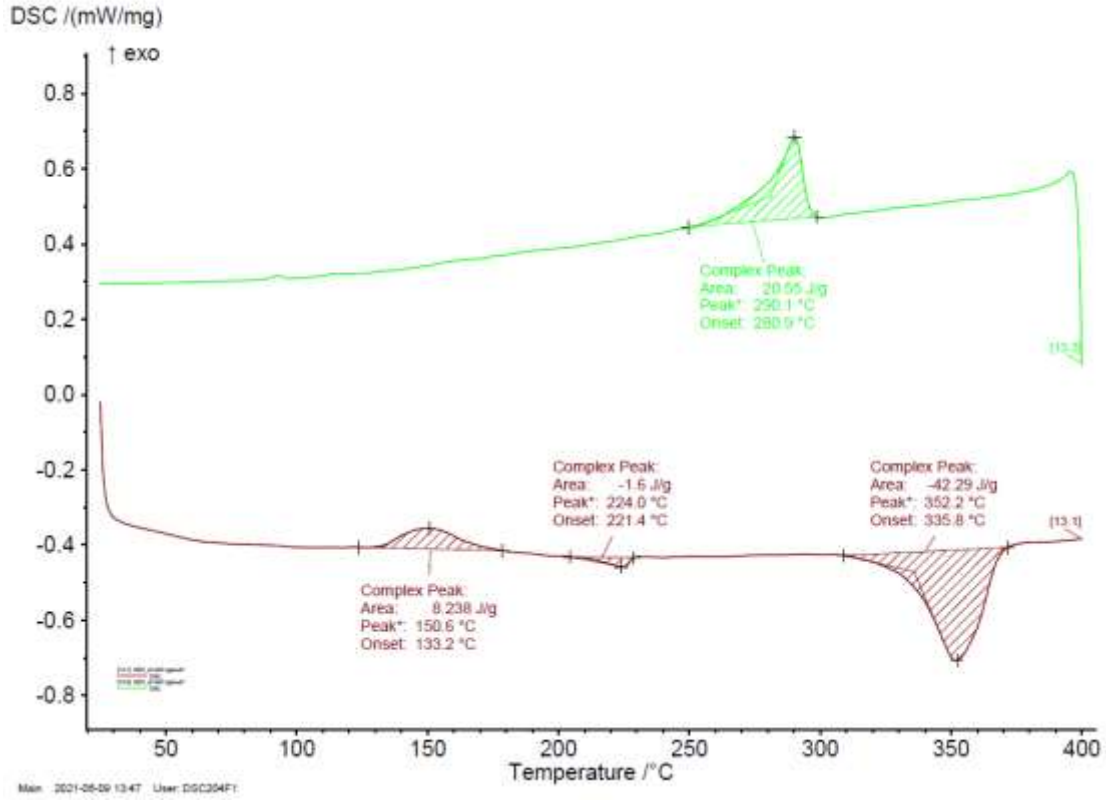

(c)

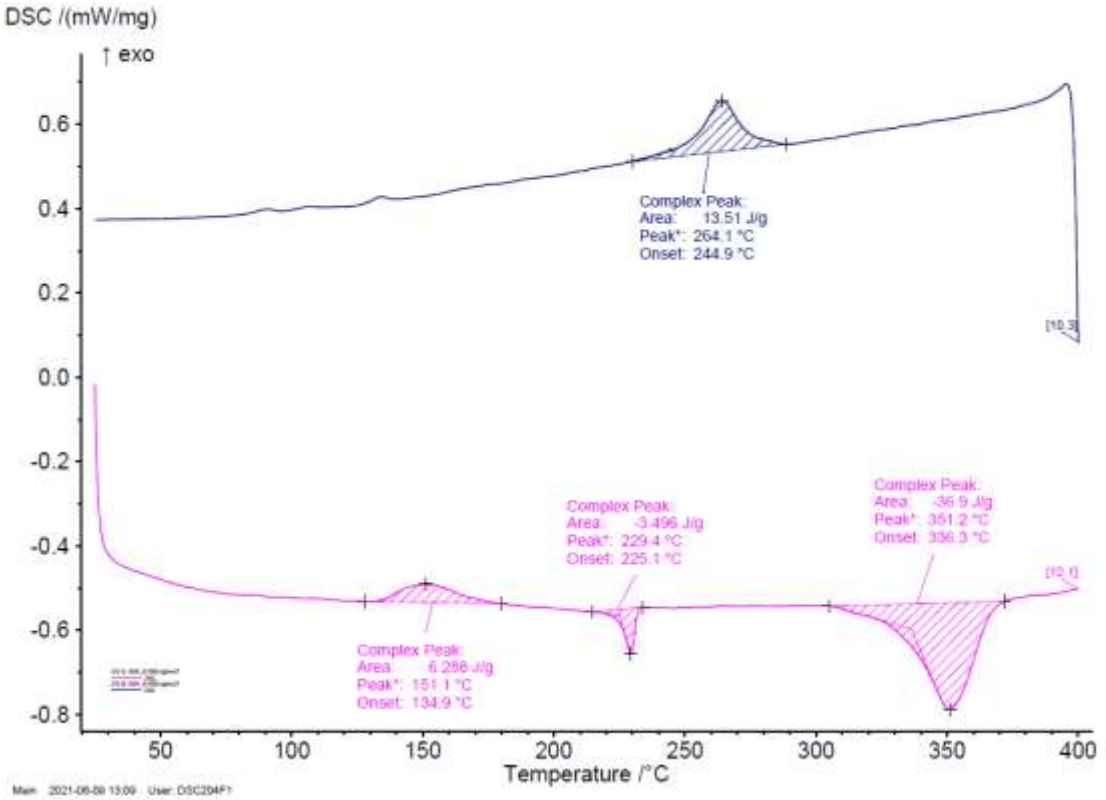

(d)

Figure 38. DSC of the PEEK composites with (a) 0 (b) 0.99 and (c) 2.31 (d) 4.95wt.% GNP after 20, 18, 15, 35h of MA respectively.

Table 4 DSC data of PEEK composites with (a) 0 (b) 0.99 and (c) 2.31 (d) 4.95wt.% GNP after 20, 18, 15, 35h of MA respectively.

	0 wt.%	0.99 wt.%	2.31 wt.%	4.95 wt.%
X_c (%)	32.58	32.75	32.53	28.38
T_m (°C)	351.6	351.0	352.2	351.2
ΔH_{cc} (J/g) - PEEK	6.49	8.225	8.238	6.288
T_{cc}(°C) –PEEK	288.2	289.9	290.1	264.1
T_{cc} (°C) -Sn-Zn-Bi	151.3	149.8	150.6	151.1

5.3. Mechanical and Tribological characterisation

5.3.1. Porosity

In order to find the optimum conditions for cold compaction different pressures and compaction times were tested and the resulting porosity of the moulds was evaluated. The results are presented in Figure 39. As is can be seen, there is a direct relationship between the pressure and porosity as well as the porosity and time. The mould produced after 5 min of cold compaction under 20MPa exhibited a rough surface with high porosity.

Higher pressure resulted in reduced porosity of the mould with a smoother finish. The same relationship was observed between compaction time and porosity. Thus parameters for cold compaction of 40MPa and a time of 15 min were selected.

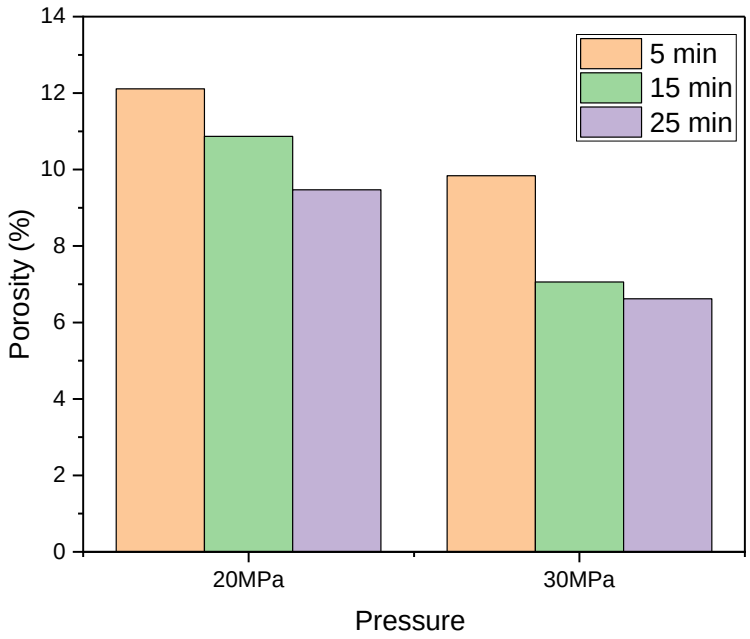

Figure 39. Porosity measurements of cold compacted composites.

5.3.2. Nanoindentation tests

The hardness (H) and reduced elastic modulus (E_r) obtained from nanoindentation tests for the samples are presented in Figure 40. These are the average values of 15 indentation tests performed on each sample. As it can be observed, the commercial PEEK exhibited the highest H and E_r values. The lowest H and E_r were observed in the pure PEEK sample obtained directly from cold compaction of raw PEEK powder. i.e., without reinforcements. It is worth mentioning that the reason for this difference is due to the samples only being cold compacted unlike commercially produced PEEK. As a result the porosity is higher and cohesion between the particles much lower, which impacts their mechanical properties.

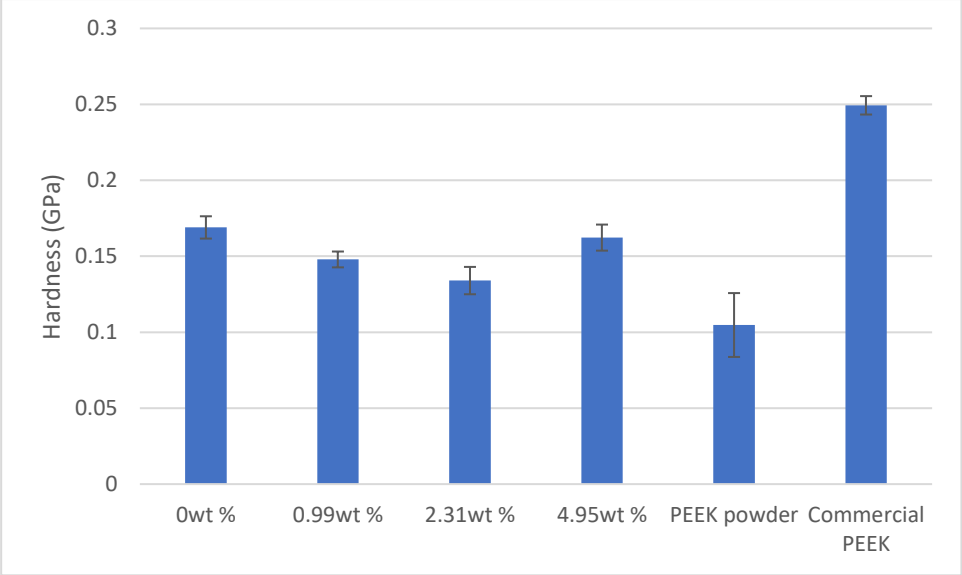

(a)

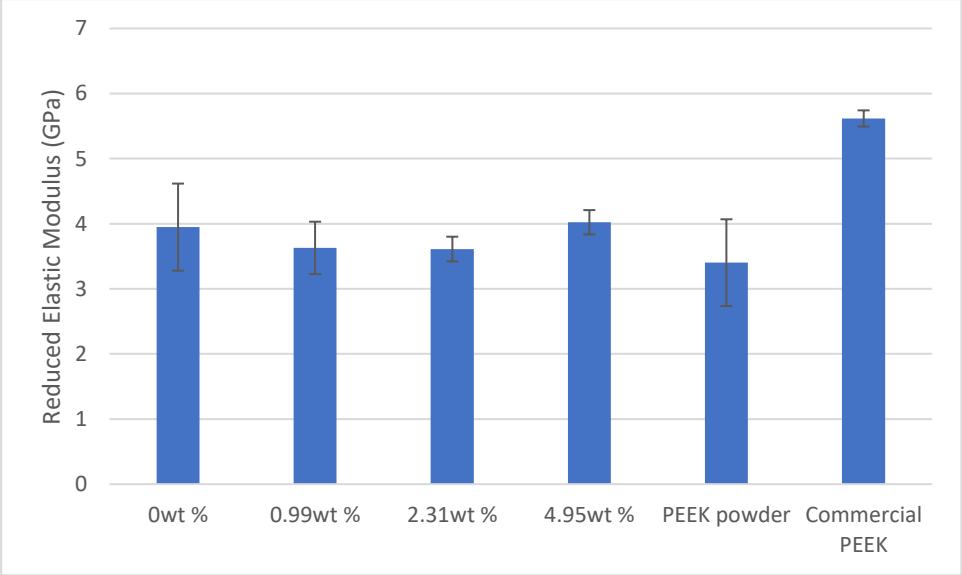

(b)

Figure 40. (a) Hardness and (b) reduced elastic modulus evaluated for all reinforced based-PEEK , PEEK and commercial PEEK samples.

Of the reinforced samples, the sample with no GNP has the highest hardness, which was only slightly higher than the sample reinforced with 4.95 wt.% GNP. Both reinforced based-PEEK samples also exhibited similar values of E_r. On the other hand, the H and E_r values show a minimum for the GNP condition of 2.31 wt.%.

This seemed to indicate that both GNP and SCF served to enhance the mechanical properties (H & E_r) of PEEK but the effect of GNP could only be observed in concentrations above 4.95wt.%. This is in agreement with the study by Molazemhosseinii et al. [49], who observed that the incorporation of carbon fibres to the PEEK matrix significantly increased the hardness and elastic modulus. On the other hand, incorporation of 0.99wt.% and 2.3wt.% of GNP reduced the H and E_r. Similar observations were made by Kalin et al. [50] , where PEEK filled with 2wt.% GNP had lower hardness than neat PEEK.

The maximum Hertzian contact pressure values between the SS balls and the six samples are presented in Figure 41. The highest contact pressure occurs between the commercial PEEK and the ball followed by pure PEEK powder. The reinforced samples exhibit similar contact pressures thus wear results will be comparable.

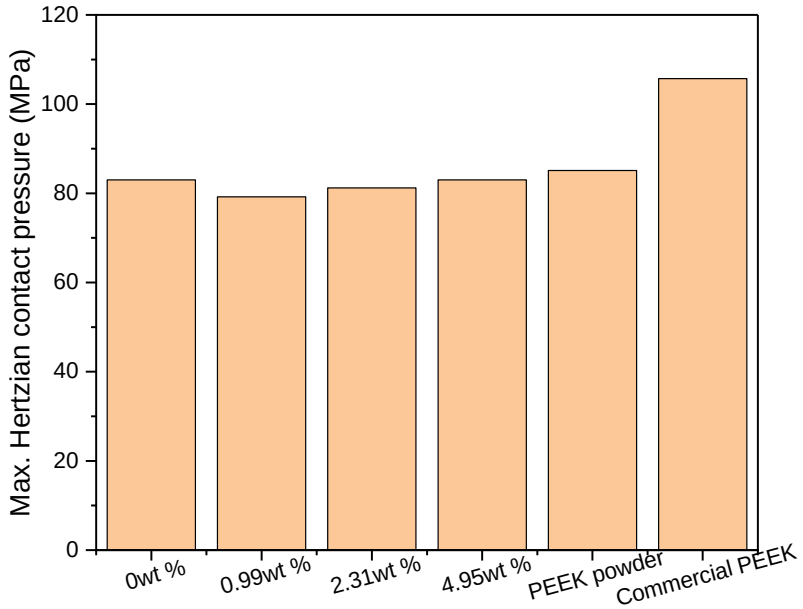

Figure 41. Max. Hertzian contact pressure between the samples and SS balls.

5.4. Morphological evaluation of worn surfaces

5.4.1. Wear morphologies of worn surfaces

Optical microscopy images of the worn samples are presented in . As can be seen, the wear tracks are characterised grooves oriented parallel to the sliding direction, with wear debris adhered to the edges of the grooves. The sample with no GNP exhibits wide (~833µm), shallow grooves. With the incorporation of 0.99wt.% GNP, the groove develops a V-shape indicative of ploughing. In addition, the width of the groove reduces to ~587 µm. Increasing the concentration of GNP to 2.31wt.%, leads to the formation of wider shallow grooves (~732µm wide) with only a small amount of wear debris on the edges.

The sample reinforced with 4.95wt.%, exhibits U-shaped grooves about ~552 µm wide. The widest wear track is observed in the PEEK powder sample (~1086µm). Furthermore, there is little to no wear debris adhered to the sides of the groove. This seems to indicate that wear occurs by a combination of abrasive and adhesive mechanisms to different extents in each sample. Similar results were observed by Kalin et al. [50]. Commercial PEEK, had the narrowest and deepest grooves ~470µm wide.

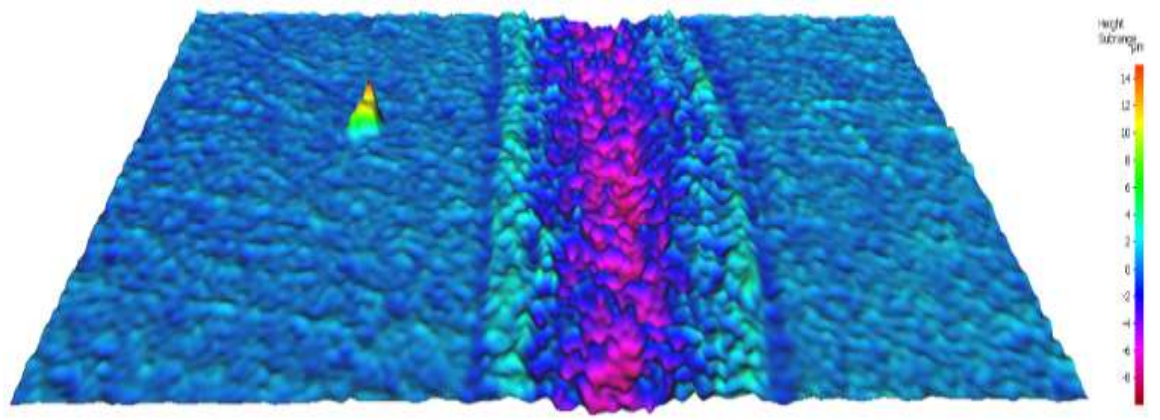

(a)

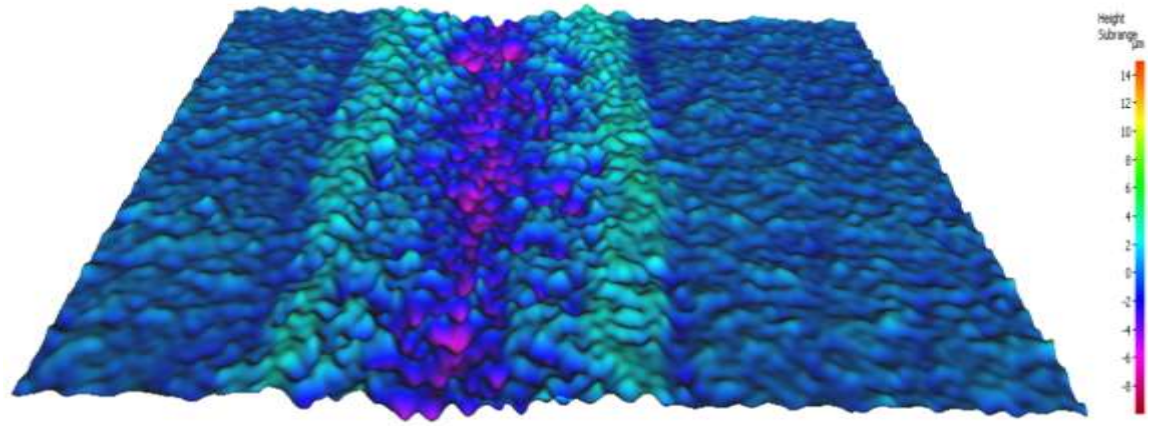

(b)

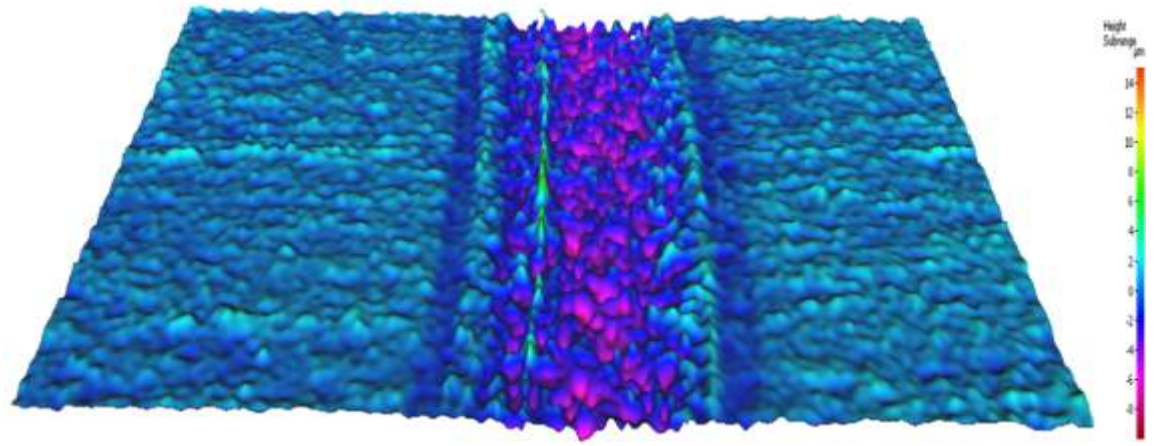

(c)

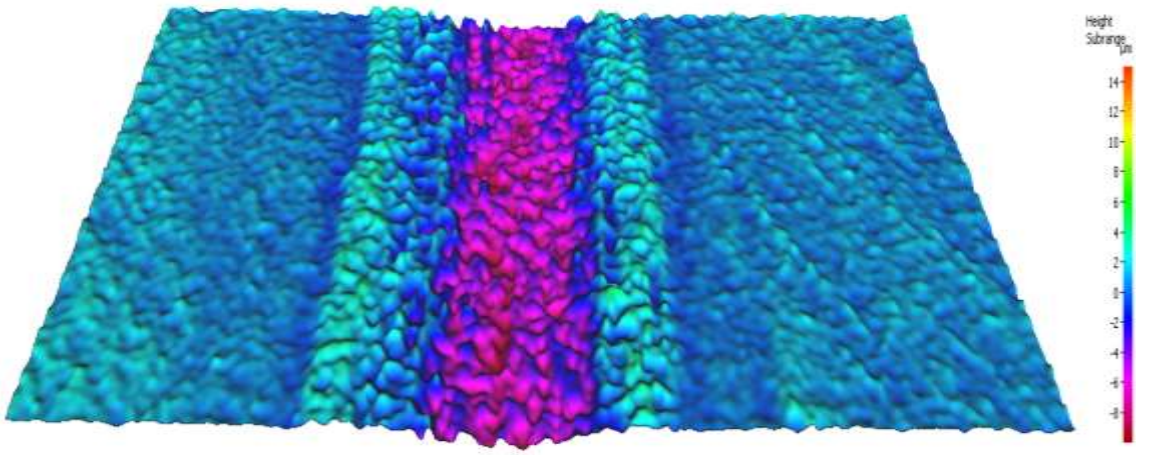

(d)

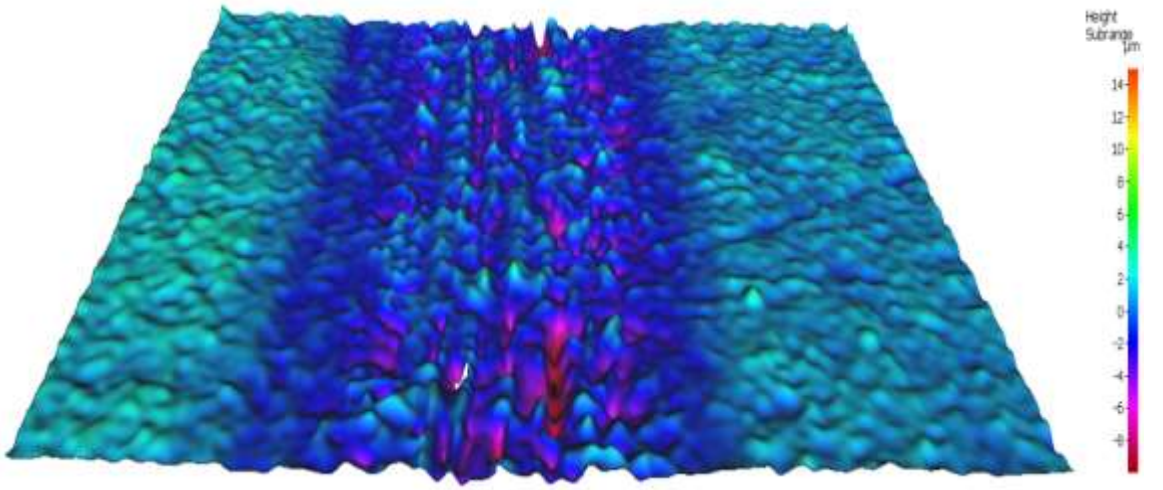

(e)

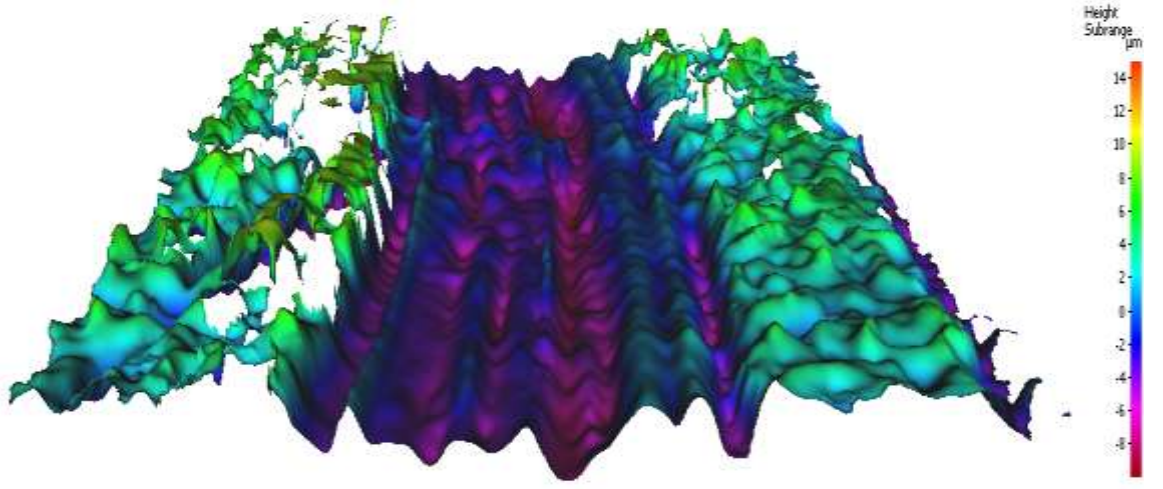

(f)

Figure 42 Optical profilometry images of worn surfaces of the samples containing (a)0 (b)0.99 (c)2.31 (d)4.95wt.% GNP (e)PEEK powder (f) Commercial PEEK

5.4.2. Wear morphologies of balls

Optical microscopy images of the worn SS balls are presented in Figure 43. Wear scratches that are oriented parallel to the sliding direction can be seen on all balls. Additionally, parts of the removed material from the disks adhered to the surface of the balls.

The transfer films with the most coverage are seen in the samples containing 0wt.%, 0.99wt.% and 2.31wt.% GNP. This explains why these balls had the lowest wear volume. The transfer film coated the surface of the ball thus delaying wear. Furthermore, the addition of GNP up to 2.31wt.%, resulted in reduced wear from the balls, which confirmed the lubricant capability of GNP. For the sample containing 4.95wt.% GNP, no transfer film was observed around the wear scar. In fact, this ball had the largest wear scar of all samples, which explains why it had the largest wear volume after commercial PEEK. Wear scars of PEEK powder and commercial PEEK were much smaller in size. In fact, the PEEK powder sample exhibited a transfer film with minimal coverage. No transfer film was formed on the ball sliding against commercial PEEK.

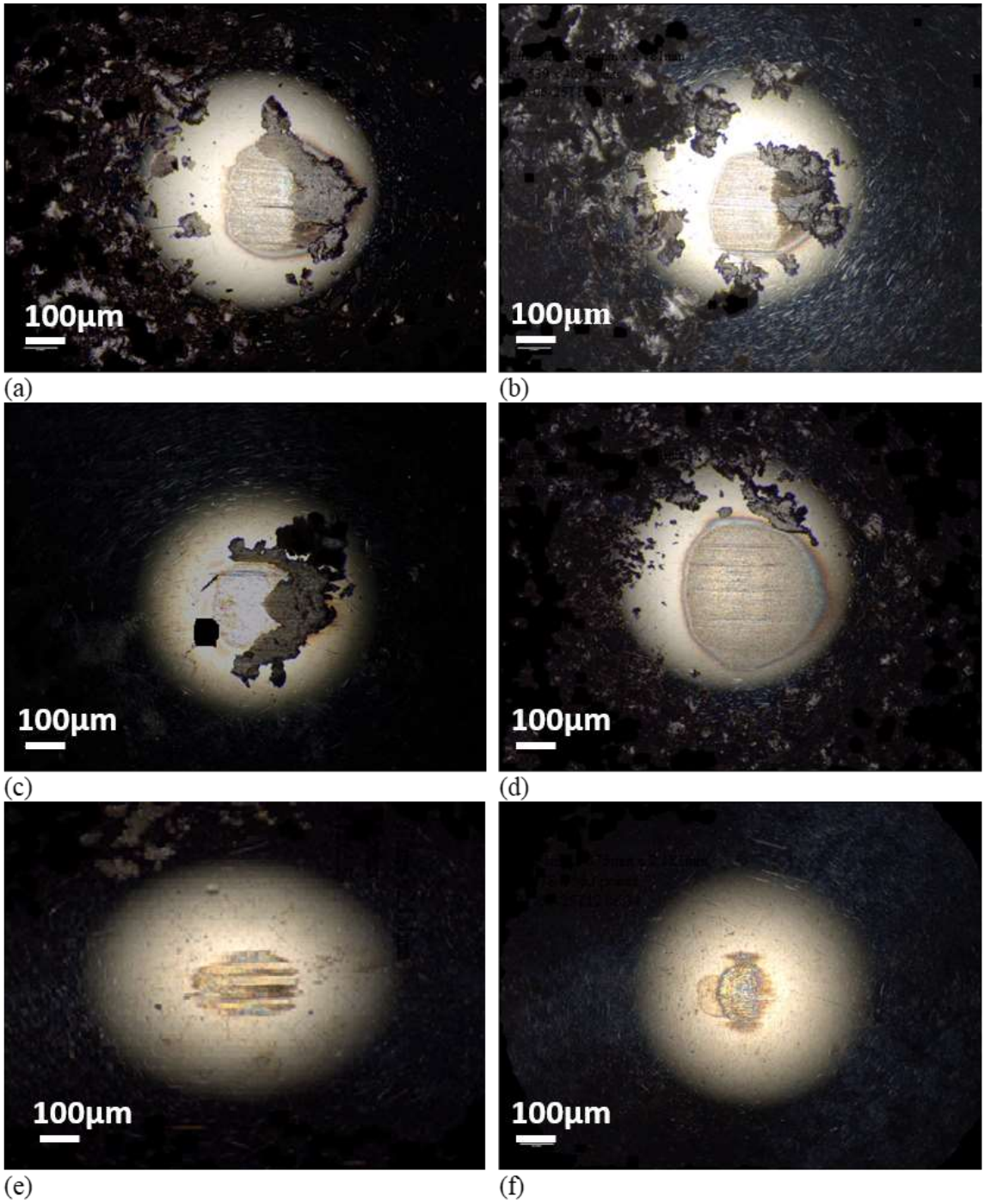

Figure 43. Optical microscopy images of the worn SS balls after sliding against the (a) 0 (b) 0.99 (c) 2.31 (d) 4.95wt.% GNP moulds € pure PEEK powder mould (f) commercial PEEK.

5.5. Tribological results

Figure 44 shows the CoF (μ) of the 6 samples comprising the compacted powders of pure PEEK, reinforced PEEK as a function of GNP percentage and commercial PEEK. As it can be seen, the recorded CoF for the pure PEEK powder sample shows an erratic profile characterised by terraces. The incorporation of both reinforcements (SCF and GNP) results in a stabilised CoF, as can be seen for the reinforced PEEK samples. The lowest static CoF value (~ 0.15) is shown by the non-reinforced PEEK powders. However, this value doesn't keep constant across the distance, but increases until it reaches a steady value of ~ 0.26 (Table 5). On the other hand, as the percentage of GNP increases, smoother, more stable profiles are recorded, which are more similar to the CoF profile shown by the commercial PEEK sample.

Furthermore, the addition of a higher percentage of GNP results in a reduction of the CoF, bringing these values closer to the commercial PEEK. Nevertheless, this trend is broken when a 2.31wt.% of GNP is added since the CoF value slightly increases from 0.32 (GNP condition of 0.99wt.%) to 0.35 and then descends to 0.28. In fact, the CoF value recorded for the GNP condition of 4.95 wt.% is almost equal to the CoF value (0.29) of the commercial PEEK.

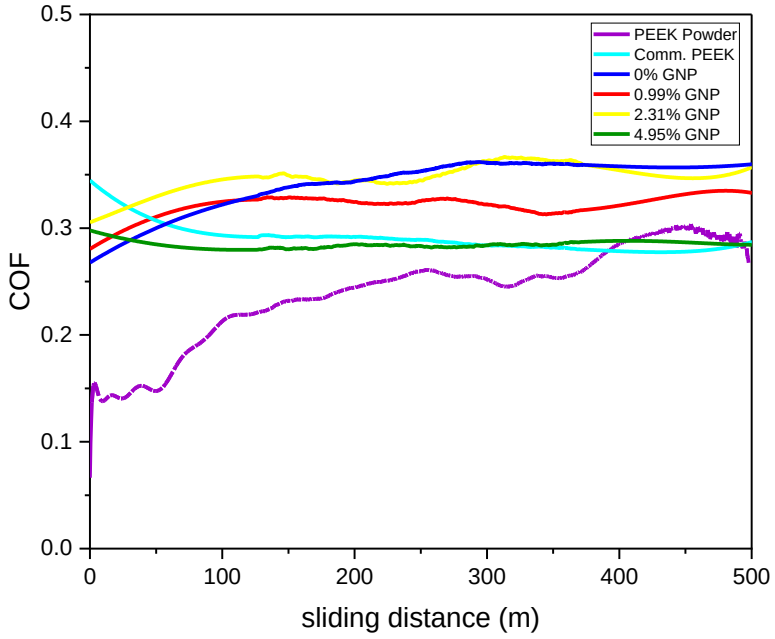

Figure 44. Evolution of CoF with journey distance for all samples.

Table 5 Average CoF of samples

Sample	CoF
0wt.% GNP	0.35
0.99wt.% GNP	0.32
2.31wt.% GNP	0.35
4.95wt.% GNP	0.28
PEEK powder	0.26
Commercial PEEK	0.29

Similar results were obtained by Puertolas et al. [15]. In their work, they showed that the CoF of GNx-PEEK composites reinforced with 5 wt.% GNP was higher than those reinforced with 3wt.% GNP, but those reinforced with 10wt.% GNP had a lower μ value [15].

In view of these results, it can be inferred that the introduction of a higher concentration of GNP is necessary to reduce friction. However, it is important to note that the reinforced PEEK samples were only cold compacted and as a result, had a certain degree of porosity around 7 %. The presence of this porosity undoubtedly modified the lubricating capacity of the GNPs, as well as the mechanical (hardness and Young's modulus) and tribological (wear volume and specific wear rate) properties.

The average wear volumes of all samples and SS balls after dry sliding at 25°C, 50% humidity are presented in Figure 45.

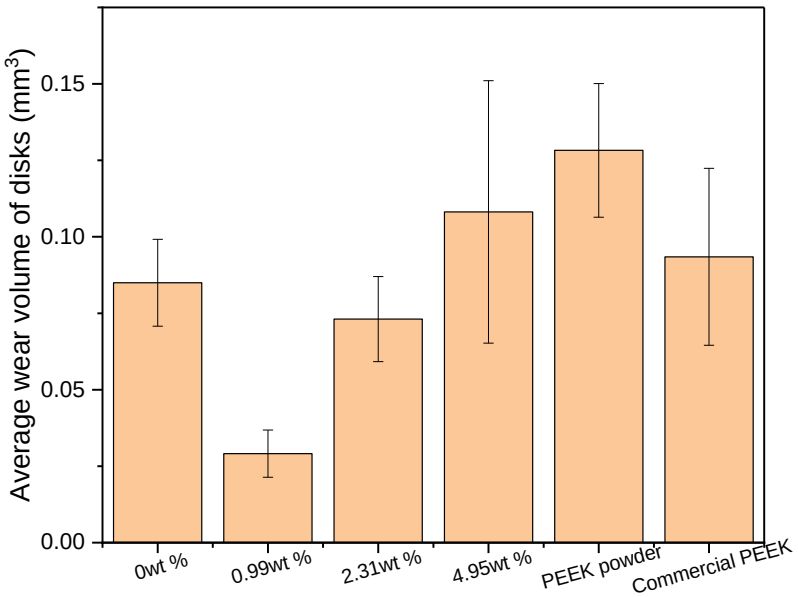

(a)

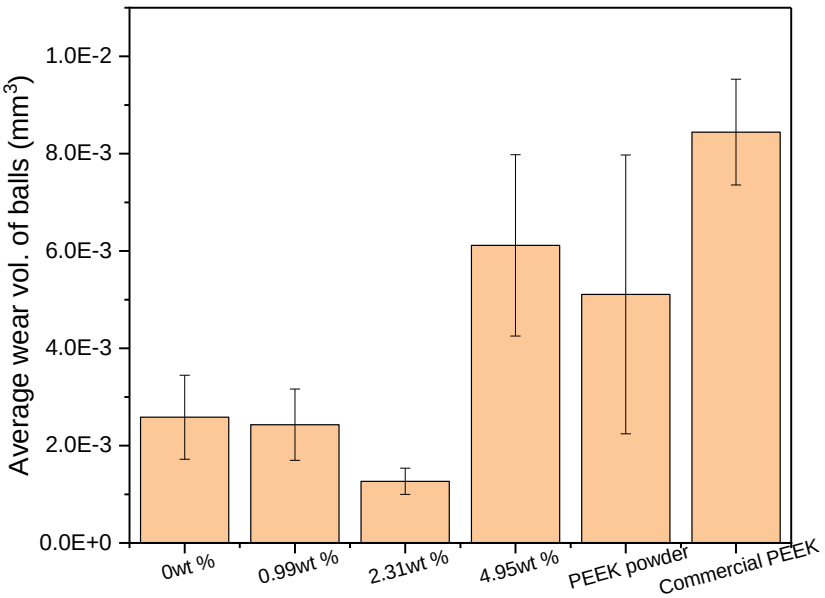

(b)

Figure 45. Average wear volume of (a) disks and (b) SS balls after dry sliding under a load (F=5N) at 25°C, 50% humidity.

It can be observed that the wear volume of the reinforced samples is lower than that of pure PEEK. This decrease might be attributed to the enhancement of hardness in the reinforced based-PEEK samples. The lowest wear volume is observed in the sample reinforced with 0.99 wt.% GNP, after which the wear volume starts to increase with increasing of GNP content. The highest wear volume is observed in the sample containing the highest content of GNP (4.95wt.%), which is even higher than that of commercial PEEK.

These results are in agreement with the study by Puertolas et al. [15], which showed that for higher concentrations of GNP (>10%), the predominant wear mechanism changes from abrasive wear to fatigue wear. This is caused by the decrease in toughness that occurs with the addition of an increasing concentration of GNP.

In the meantime, significantly low wear is observed from the balls of the reinforced samples up to 2.31wt.%. When GNP content is increased to 4.95wt.%, the wear volume of the balls significantly increases even higher than that against the pure PEEK powder sample. The highest wear volume is observed in the ball sliding against commercial PEEK.

The specific wear rates (k) of the samples and their respective balls are presented in Figure 46. As it can be seen, the sample obtained from the cold compaction of raw PEEK powder experienced the lowest wear resistance. The specific wear rate is observed to be lower for the reinforced based-PEEK samples compared to the sample compacted from raw PEEK powder. A significantly high wear resistance is observed when PEEK powder is reinforced with 0.99 wt.% GNP, which is four times lower compared to the sample compacted from raw PEEK powder. With increasing GNP content (4.95 wt.%), k is observed to increase and it gets even higher than that of the sample with no GNP. Commercial PEEK exhibits a similar sliding resistance to that of the sample with 0wt.% GNP.

In the meantime, the ball sliding against commercial PEEK experienced significantly high k. This can be attributed to the significantly high hardness of commercial PEEK. The balls sliding against the reinforced PEEK samples exhibit much lower values of k, which decrease with the incorporation of up to 2.31 wt.% GNP. However, when GNP content is increased to 4.95 wt.% the specific wear rate of the ball increases five times higher than that of 2.31 wt.%.

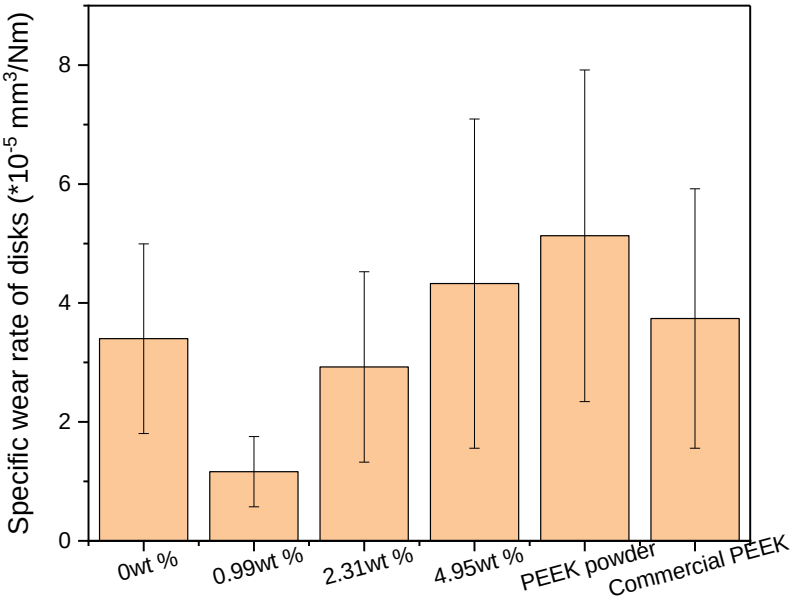

(a)

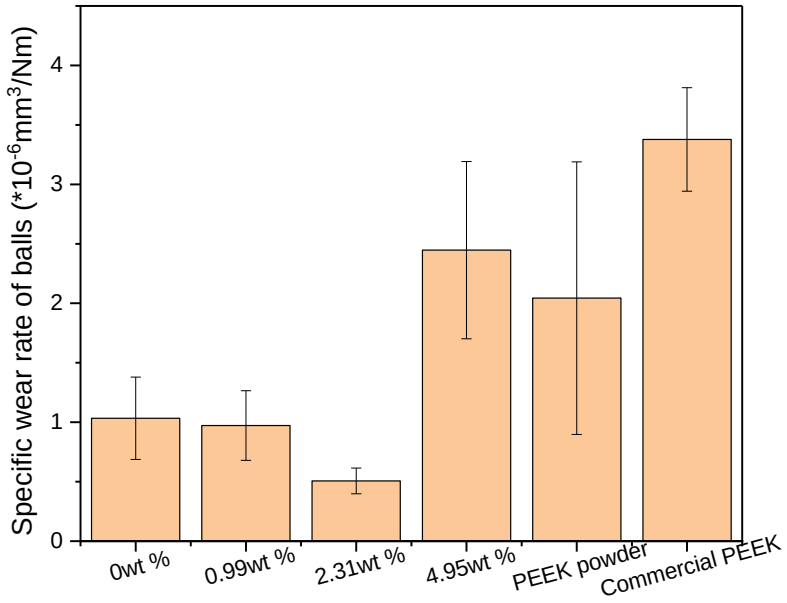

(b)

Figure 46. Specific wear rates of (a) disks (b) SS balls after dry sliding after dry sliding under a load (F=5N) at 25°C, 50% humidity.

6. Conclusion

Four composite mixtures composed of 67wt.% of PEEK and 33wt.% of reinforcements were made by MA, where the total content of GNP was varied between; 0 , 0.99, 2.31 and 4.95wt.%. The composites were cold compacted to produced moulds and their mechanical, structural and tribological properties evaluated against those of pure PEEK and commercial PEEK.

The results obtained in the studies can be summarised as follows:

The incorporation of the Sn-Zn-Bi brazing alloy, SCF and GNP had a positive effect on the mechanical properties of PEEK. The reinforced PEEK samples exhibited increased hardness and Young's modulus against pure PEEK powder. Of the samples containing GNP, a decrease in hardness and Young's Modulus was observed when GNP was increased from 0.99 to 2.31wt.%. However, at the highest concentration, these values increased and were similar to those of the sample with no GNP. This seemed to indicate that both GNP and SCF served to enhance the mechanical properties (H & E_r) of PEEK but the effect of GNP could only be observed in concentrations above 4.95wt.%.

Commercial PEEK still had significantly higher mechanical properties but since these composites were only cold compacted, this was expected.

Reinforced PEEK showed a higher COF than pure PEEK powder (~0.35, ~0.32, ~0.35, ~0.28) for 0 , 0.99, 2.31 and 4.95wt.% GNP respectively. However increasing the concentration of GNP to 4.95wt.% significantly reduced the COF to a value close to that of pure PEEK powder and commercial PEEK (~0.26 and ~0.29 respectively). No linear relationship between the GNP content and CoF could be established.

GNP had an effect on the crystallinity of the sample. With the addition of 0.99wt.% of GNP a slight increase in crystallinity was observed. However increasing the concentration of GNP caused a reduction in crystallinity.

Significantly lower wear volumes and wear rates were observed in the reinforced samples up to 2.31wt.% GNP. The lowest wear was observed when the sample was reinforced with 0.99wt.% GNP which was four times lower than that of the pure PEEK powder and three times lower than commercial PEEK. Transfer films from the removed materials on these samples were observed on the balls which were responsible for this reduction in wear.

Additionally significantly low wear volumes and wear rates were observed in the balls sliding against the reinforced samples up to 2.31wt.% GNP. This were in the order of two times lower than pure PEEK and four times lower than commercial PEEK. At higher concentration of GNP (4.95wt.%) the wear rate of the balls increases by a factor of five.

From the research that has been carried out, it is possible to conclude that the reinforcement of PEEK with the Sn-Zn-Bi brazing alloy, SCF and GNP had positive results. However it is important to consider the tailoring of the GNP concentration to obtain the best results.

7. Further research

On the basis of the promising findings presented in this project, further study would be of interest.

Heat treatment of the samples should be considered in the future to reduce the porosity of the samples, so that the results can be comparable to commercial PEEK.

Additionally, the initial production technique based on the texturing of PEEK polymer and introducing and sintering of the reinforcement into the grooves produced may be considered in future projects. Preliminary experiments were carried out at the University of Aveiro in which a 355 nm UV laser with 10 passes at a velocity of 100 mm/s and a groove width of 90 μm was used to texture the surface of PEEK.

The 3D profilometry results of LST of PEEK showed positive results as can be seen in Figure 47. The pattern produced consisted of regular groove patterns with an average width of 90 μm and depths ranging from 70-90 μm. It was expected that increasing the number of passes from 10 to 15, using the same velocity and width, would bring the depth values of the groove closer to the intended depth of 100 and 150 μm.

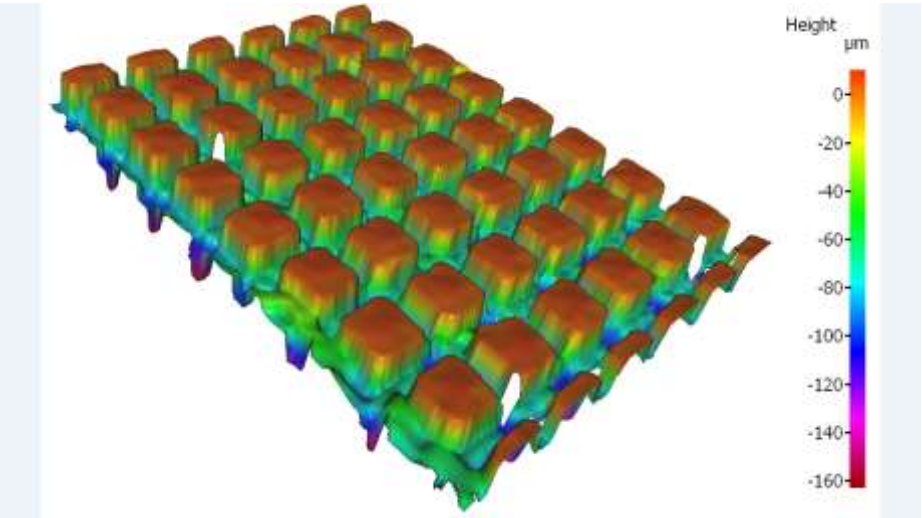

(a)

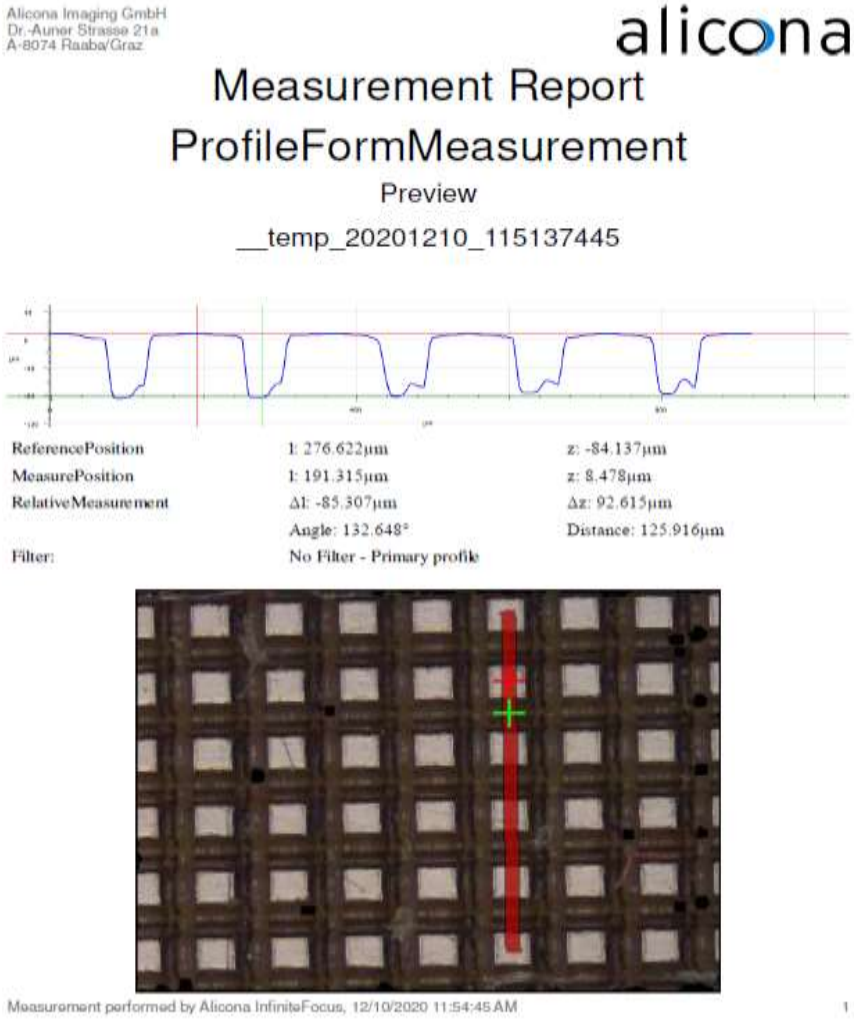

(b)

Figure 47. Confocal microscope image of textured PEEK after 10 passes at 100 mm/s with UV 355nm pulsed laser (b) Surface profile measurement of textured profile.

8. References

[1] C. Huynh *et al.*, "Factors associated with the orthopaedic surgeon's decision to recommend total joint replacement in hip and knee osteoarthritis: an international cross-sectional study of 1905 patients," *Osteoarthritis and cartilage,* vol. 26, no. 10, pp. 1311-1318, 2018, doi: 10.1016/j.joca.2018.06.013.

[2] S. B. Goodman, M. A. Wimmer, and H. L. Ploeg, "Recent advances in total joint replacement," *Journal of orthopaedic research,* vol. 38, no. 7, pp. 1413-1413, 2020, doi: 10.1002/jor.24734.

[3] Y.-G. Koh, K.-M. Park, J.-A. Lee, J.-H. Nam, H.-Y. Lee, and K.-T. Kang, "Total knee arthroplasty application of polyetheretherketone and carbon-fiber-reinforced polyetheretherketone: A review," *Materials Science & Engineering C,* vol. 100, pp. 70-81, 2019, doi: 10.1016/j.msec.2019.02.082.

[4] W. M. Mihalko, H. Haider, S. Kurtz, M. Marcolongo, and K. Urish, "New materials for hip and knee joint replacement: What's hip and what's in kneed?," *Journal of orthopaedic research,* vol. 38, no. 7, pp. 1436-1444, 2020, doi: 10.1002/jor.24750.

[5] A. A. Stratton-Powell, K. M. Pasko, C. L. Brockett, and J. L. Tipper, "The Biologic Response to Polyetheretherketone (PEEK) Wear Particles in Total Joint Replacement: A Systematic Review," Clin Orthop Relat Res, vol. 474, pp. 2394–2404, 2016, doi: 10.1007/s11999-016-4976-z.

[6] J. Song *et al.*, "Insight into the wear particles of PEEK and CFRPEEK against UHMWPE for artificial cervical disc application: Morphology and immunoreaction," *Tribology international,* vol. 144, pp. 106093, 2020, doi: 10.1016/j.triboint.2019.106093.

[7] N. Kumar, N. C. Arora, and B. Datta, "Bearing surfaces in hip replacement – Evolution and likely future," *Medical Journal Armed Forces India,* vol. 70, no. 4, pp. 371-376, 2014/10/01/ 2014, doi: 10.1016/j.mjafi.2014.04.015.

[8] E. Peltola *et al.*, "Materials used for hip and knee implants," 2013, pp. 178-218.

[9] S. W. King, J. M. Royeca, C. M. Cunningham, R. Madegowda, S. Sha, and H. Pandit, "Metal hypersensitivity in total knee arthroplasty," *Journal of Arthroscopy and Joint Surgery,* vol.7,pp. 184-188, 2020, doi: 10.1016/j.jajs.2020.09.004.

[10] M. Lyasaght, T. Webster, *Biomaterials for artificial organs* (Woodhead Publishing in materials). Cambridge, UK ;: Woodhead Pub., 2011.

[11] E. Oral, "3 - Polymeric joint bearing surfaces for total joint replacements," in *Biomaterials for Artificial Organs*, M. Lysaght and T. J. Webster Eds.: Woodhead Publishing, 2011, pp. 56-80.

[12] E. Kaivosoja *et al.*, "7 - Materials used for hip and knee implants," in *Wear of Orthopaedic Implants and Artificial Joints*, S. Affatato Ed.: Woodhead Publishing, 2013, pp. 178-218.

[13] M. Hedayati, M. Salehi, R. Bagheri, M. Panjepour, and A. Maghzian, "Ball milling preparation and characterisation of poly (ether ether ketone)/surface modified silica nanocomposite," *Powder Technology,* vol. 207, no. 1, pp. 296-303, 2011/02/15/ 2011, doi: 10.1016/j.powtec.2010.11.011.

[14] X. Lv *et al.*, "Incorporation of molybdenum disulfide into polyetheretherketone creating biocomposites with improved mechanical, tribological performances and cytocompatibility for artificial joints applications," *Colloids and surfaces, B, Biointerfaces,* vol. 189, pp. 110819-110819, 2020, doi: 10.1016/j.colsurfb.2020.110819.

[15] J. A. Puértolas, M. Castro, J. A. Morris, R. Ríos, and A. Ansón-Casaos, "Tribological and mechanical properties of graphene nanoplatelet/PEEK composites," *Carbon (New York),* vol. 141, pp. 107-122, 2019, doi: 10.1016/j.carbon.2018.09.036.

[16] O. Khayal, *MANUFACTURING AND PROCESSING OF COMPOSITE MATERIALS*. 2019, doi: 10.13140/RG.2.2.30822.57928.

[17] M. Jawaid and M. Thariq, “12. Potential of Natural Fiber/Biomass Filler-Reinforced Polymer Composites in Aerospace Applications,” in *Sustainable Composites for Aerospace Applications*: Elsevier, 2018.
[18] H. W. Toh *et al.*, “Polymer blends and polymer composites for cardiovascular implants,” *European Polymer Journal,* vol. 146, p. 110249, 2021/03/05/ 2021, doi: 10.1016/j.eurpolymj.2020.110249.
[19] B. Chen, S. Berretta, R. Davies, and O. Ghita, “Characterisation of carbon fibre (Cf) - Poly Ether Ketone (PEK) composite powders for laser sintering,” *Polymer testing,* vol. 76, pp. 65-72, 2019, doi: 10.1016/j.polymertesting.2019.03.011.
[20] M. Fahim, N. Chand, “2 - Introduction to tribology of polymer composites,” in *Tribology of Natural Fiber Polymer Composites*, N. Chand and M. Fahim Eds.: Woodhead Publishing, 2008, pp. 59-83.
[21] G. Kandemir, S. Smith, and T. J. Joyce, “Wear behaviour of CFR PEEK articulated against CoCr under varying contact stresses: Low wear of CFR PEEK negated by wear of the CoCr counterface,” *Journal of the mechanical behavior of biomedical materials,* vol. 97, pp. 117-125, 2019, doi: 10.1016/j.jmbbm.2019.05.022.
[22] D. Bhattacharyya and S. Fakirov, “1. Manufacturing and Processing of Polymer Composites,” in *Synthetic Polymer-Polymer Composites*: Hanser Publishers, 2012.
[23] J. Song, Y. H. Liu, S. Wang, Z. H. Liao, and W. Q. Liu, “Study on the wettability and tribological behaviors of glass fiber reinforced poly(ether-ether-ketone) against different polymers as bearing materials for artificial cervical disc,” *Biotribology (Oxford),* vol. 4, pp. 18-29, 2015, doi: 10.1016/j.biotri.2015.10.001.
[24] D. Cordero, M. Lopez-Alvarez, C. Rodriguez-Valencia, J. Serra, S. Chiussi, and P. Gonzalez, “In vitro response of pre-osteoblastic cells to laser microgrooved PEEK,” *Biomedical materials (Bristol),* vol. 8, no. 5, p. 055006, 2013, doi: 10.1088/1748-6041/8/5/055006.
[25] J. Song *et al.*, “In vitro wear study of PEEK and CFRPEEK against UHMWPE for artificial cervical disc application,” *Tribology international,* vol. 122, pp. 218-227, 2018, doi: 10.1016/j.triboint.2018.02.034.
[26] S. Thomas, M. Hosur, and C. J. Chirayil, “4.6 Detailed Overview of Nanofillers,” in *Unsaturated Polyester Resins - Fundamentals, Design, Fabrication, and Applications*: Elsevier, 2019.
[27] O. H. Wang, Q. J. Xue, and W. C. Shen, “The friction and wear properties of nanometre SiO2 filled polyetheretherketone,” *Tribology international,* vol. 30, no. 3, pp. 193-197, 1997, doi: 10.1016/S0301-679X(96)00042-4.
[28] M. S. El-Eskandarany, *Mechanical alloying for fabrication of advanced engineering materials*. Norwich, N.Y: Noyes Publications/W. Anderew Pub., 2001.
[29] J. Pan and W. J. D. Shaw, “Effects of processing parameters on material properties of mechanically processed polyamide,” *Journal of Applied Polymer Science,* https://doi.org/10.1002/app.1995.070560504 vol. 56, no. 5, pp. 557-566, 1995/05/02 1995, doi: 10.1002/app.1995.070560504.
[30] P. R. Monich, B. Henriques, A. P. Novaes de Oliveira, J. C. M. Souza, and M. C. Fredel, “Mechanical and biological behavior of biomedical PEEK matrix composites: A focused review,” *Materials letters,* vol. 185, pp. 593-597, 2016, doi: 10.1016/j.matlet.2016.09.005.
[31] S. Javaid, M. Dey, N. Kaabouch, and S. Gupta, “On the potential of polyetheretherketone matrix composites reinforced with ternary nanolaminates for tribological and biomedical applications,” *Journal of applied polymer science,* vol. 138, no. 10, p. n/a, 2021, doi: 10.1002/app.49980.
[32] X. Gu, Y. Zheng, Y. Cheng, S. Zhong, and T. Xi, “In vitro corrosion and biocompatibility of binary magnesium alloys,” *Biomaterials,* vol. 30, no. 4, pp. 484-498, 2009/02/01/ 2009, doi: 10.1016/j.biomaterials.2008.10.021.

[33] Z. Zhen, T. Xi, Y. Zheng, L. Li, and L. Li, "In Vitro Study on Mg–Sn–Mn Alloy as Biodegradable Metals," *Journal of Materials Science & Technology,* vol. 30, no. 7, pp. 675-685, 2014/07/01/ 2014, doi: 10.1016/j.jmst.2014.04.005.

[34] M. E. Moussa, H. I. Mohamed, M. A. Waly, G. S. Al-Ganainy, A. B. Ahmed, and M. S. Talaat, "Comparison study of Sn and Bi addition on microstructure and bio-degradation rate of as-cast Mg-4wt% Zn alloy without and with Ca-P coating," *Journal of Alloys and Compounds,* vol. 792, pp. 1239-1247, 2019/07/05/ 2019, doi: 10.1016/j.jallcom.2019.03.363.

[35] G. K. Levy, J. Goldman, and E. Aghion, "The Prospects of Zinc as a Structural Material for Biodegradable Implants-A Review Paper," *Metals (Basel),* vol. 7, no. 10, p. 402, 2017, doi: 10.3390/met7100402.

[36] S. Prasad S *et al.*, "In vitro bioactivity and antibacterial properties of bismuth oxide modified bioactive glasses," *Journal of materials research,* vol. 33, no. 2, pp. 178-190, 2018, doi: 10.1557/jmr.2017.442.

[37] R. Goyal, Y. S. Negi, and A. Tiwari, "High performance polymer composites on PEEK reinforced with aluminum oxide," *Journal of Applied Polymer Science,* vol. 100, pp. 4623-4631, 06/15 2006, doi: 10.1002/app.23083.

[38] J. S. Benjamin, "Mechanical alloying — A perspective," *Metal powder report,* vol. 45, no. 2, pp. 122-127, 1990, doi: 10.1016/s0026-0657(10)80124-9.

[39] O. D. Neikov, "Chapter 3 - Mechanical Alloying," *Handbook of Non-Ferrous Metal Powders*, pp. 63-79, 2nd ed: Elsevier Science & Technology, 2018.

[40] P. S. Gilman and J. S. Benjamin, "Mechanical Alloying," *Annual review of materials science,* vol. 13, no. 1, pp. 279-300, 1983, doi: 10.1146/annurev.ms.13.080183.001431.

[41] V. Baheti, A. M. R. Abbasi, and J. Militky, "Ball milling of jute fibre wastes to prepare nanocellulose," *World Journal of Engineering,* vol. 9, pp. 45-50, 02/03 2012, doi: 10.1260/1708-5284.9.1.45.

[42] Y. Niu, S. Zheng, P. Song, X. Zhang, and C. Wang, "Mechanical and thermal properties of PEEK composites by incorporating inorganic particles modified phosphates," *Composites Part B: Engineering,* vol. 212, p. 108715, 2021/05/01/ 2021, doi: 10.1016/j.compositesb.2021.108715.

[43] S. Utzschneider *et al.*, "Inflammatory response against different carbon fiber-reinforced PEEK wear particles compared with UHMWPE in vivo," *Acta biomaterialia,* vol. 6, no. 11, pp. 4296-4304, 2010, doi: 10.1016/j.actbio.2010.06.002.

[44] W. C. Oliver and G. M. Pharr, "An improved technique for determining hardness and elastic modulus using load and displacement sensing indentation experiments," *Journal of Materials Research,* vol. 7, no. 6, pp. 1564-1583, 1992, doi: 10.1557/JMR.1992.1564.

[45] S. Kucharski and Z. Mróz, "Identification of wear process parameters in reciprocating ball-on-disc tests," *Tribology International,* vol. 44, no. 2, pp. 154-164, 2011/02/01/ 2011, doi: 10.1016/j.triboint.2010.10.010.

[46] H. Zhang, W.-M. Tang, G.-Q. Xu, Y.-C. Wu, and Z.-X. Zheng, "Synthesis of Sn–Ag binary alloy powders by mechanical alloying," *Materials Chemistry and Physics,* vol. 122, no. 1, pp. 64-68, 2010/07/01/ 2010, doi: 10.1016/j.matchemphys.2010.02.075.

[47] M. L. Huang, C. M. L. Wu*, J. K. L. Lai, L. Wang, and F. G. Wang, "Lead free solder alloys Sn-Zn and Sn-Sb prepared by mechanical alloying," *Journal of Materials Science: Materials in Electronics,* vol. 11, no. 1, pp. 57-65, 2000/02/01 2000, doi: 10.1023/A:1008908321027.

[48] A. E. Brink, K. J. Jordens, and J. S. Riffle, "Sintering high performance semi-crystalline polymeric powders," *Polymer Engineering & Science,* https://doi.org/10.1002/pen.760352403 vol. 35, no. 24, pp. 1923-1930, 1995/12/01 1995, doi: 10.1002/pen.760352403.

[49] A. Molazemhosseini, H. Tourani, M. R. Naimi-Jamal, and A. Khavandi, "Nanoindentation and nanoscratching responses of PEEK based hybrid composites reinforced with short carbon

fibers and nano-silica," *Polymer Testing,* vol. 32, no. 3, pp. 525-534, 2013/05/01/ 2013, doi: https://doi.org/10.1016/j.polymertesting.2013.02.001.

[50] M. Kalin, M. Zalaznik, and S. Novak, "Wear and friction behaviour of poly-ether-ether-ketone (PEEK) filled with graphene, WS2 and CNT nanoparticles," *Wear,* vol. 332-333, pp. 855-862, 2015/05/01/ 2015, doi: https://doi.org/10.1016/j.wear.2014.12.036.